Descending locus coeruleus noradrenergic signaling to spinal astrocyte subset is required for stress-induced pain facilitation

Riku Kawanabe-Kobayashi[1,8], Sawako Uchiyama[1,8], Kohei Yoshihara[1,8], Daiki Kojima[1], Thomas McHugh[2], Izuho Hatada[3,4], Ko Matsui[5], Kenji F. Tanaka[6], Makoto Tsuda[1,7,*]

Affiliations

[1]Department of Molecular and System Pharmacology, Graduate School of Pharmaceutical Sciences, Kyushu University, 3-1-1 Maidashi, Higashi-ku, Fukuoka 812-8582, Japan

[2]Laboratory for Circuit and Behavioral Physiology, RIKEN Center for Brain Science, 2-1 Hirosawa, Wako, Saitama 351-0198, Japan

[3]Laboratory of Genome Science, Biosignal Genome Resource Center, Institute for Molecular and Cellular Regulation, Gunma University, 3-39-15 Showa-machi, Maebashi, Gunma 371-8512, Japan

[4]Viral Vector Core, Gunma University Initiative for Advanced Research (GIAR), 3-39-22, Showa-machi, Maebashi, Gunma, 371-8511, Japan

[5]Super-network Brain Physiology, Graduate School of Life Sciences, Tohoku University, 2-1-1 Katahira, Aoba-ku, Sendai, Miyagi 980-8577, Japan

[6]Division of Brain Sciences, Institute for Advanced Medical Research, Keio University School of Medicine, 35 Shinanomachi, Shinjuku-ku, Tokyo 160-8582, Japan

[7]Kyushu University Institute for Advanced Study, 744 Motooka, Nishi-ku, Fukuoka 819-0395, Japan

[8]These authors contributed equally.

*Correspondence: Makoto Tsuda, Ph.D.; **TEL:** 81-92-642-6628, **FAX:** 81-92-642-6566, **Email:** tsuda@phar.kyushu-u.ac.jp

Abstract

It is known that stress powerfully alters pain, but its underlying mechanisms remain elusive. Here, we identified a circuit, locus coeruleus descending noradrenergic neurons projecting to the spinal dorsal horn ($LC^{\rightarrow SDH}$-NA neurons), that is activated by acute exposure to restraint stress and is required for stress-induced mechanical pain hypersensitivity in mice. Interestingly, the primary target of spinal NA released from descending $LC^{\rightarrow SDH}$-NAergic terminals causing the stress-induced pain hypersensitivity was α_{1A}-adrenaline receptors (α_{1A}Rs) in Hes5-positive ($Hes5^{+}$) astrocytes located in the SDH, an astrocyte subset that has an ability to induce pain sensitization. Furthermore, activation of $Hes5^{+}$ astrocytes reduced activity of SDH-inhibitory neurons (SDH-INs) that have an inhibitory role in pain processing. This astrocytic reduction of IN activity was canceled by an A_1-adenosine receptor (A_1R)-knockdown in SDH-INs, and the A_1R-knockdown suppressed pain hypersensitivity caused by acute restraint stress. Therefore, our findings suggest that $LC^{\rightarrow SDH}$-NA neuronal signaling to $Hes5^{+}$ SDH astrocytes and subsequent astrocytic reduction of SDH-IN activity are essential for pain facilitation caused by stress.

Introduction

Somatosensory information generated at the periphery, such as skin, is conveyed to the dorsal horn of the spinal cord (SDH) via primary afferent sensory neurons and further to the brain[1,2]. The SDH is the first region for processing the peripherally derived sensory information and thus is critical for its proper transmission to and perception in the brain[1-6]. The processing of somatosensory information is not only tightly regulated by complex neuronal circuits within the SDH but also powerfully modulated by descending neurons from the brain[7,8]. The locus coeruleus (LC), a small nucleus located in the brainstem, modulates pain information processing in the SDH via descending noradrenaline (NA) neurons[8-11]. Activation of SDH-projecting LC-NA ($LC^{\rightarrow SDH}$-NA) neurons leads to a release of NA in the SDH[12]. Spinal NA acts on α_{1A}-adrenaline receptors (α_{1A}Rs) expressed on inhibitory neurons (INs)[13,14] and facilitates γ-aminobutyric acid (GABA)-mediated inhibitory synaptic transmission[15,16]. This NA signal has been implicated in the inhibitory control of nociceptive information processing[9-11]. Besides neurons, glial cells in the SDH, such as microglia and astrocytes, also have a remarkable ability to modulate the processing and transmission of somatosensory information[17-19]. Glial modulation has been extensively studied in pathological settings[17-19], but studies using *in vivo* imaging have shown that SDH astrocytes respond to noxious stimuli applied to the periphery under normal conditions[20-23]. Furthermore, we have recently identified a subset of spinal astrocytes defined by expression of hairy and enhancer of split 5 (Hes5) as a new target of NA[22]. Astrocytes express various types of adrenaline receptors[24]; activation of $LC^{\rightarrow SDH}$-NA neurons induces an increase in intracellular Ca^{2+} ($[Ca^{2+}]_i$), an indicator of astrocyte activity[25], via α_{1A}Rs[22], which are the most abundant adrenaline receptors in astrocytes[26,27]. $Hes5^+$ astrocytes are selectively distributed in the superficial laminae of SDH where it receives primary afferent sensory fibers. Activation of α_{1A}Rs of $Hes5^+$ SDH astrocytes by intrathecal administration of NA induces pain sensitization to light mechanical stimuli applied to the skin[22]. Given that most of the varicosities of NAergic axons/terminals are located closer to astrocytic processes than to neuronal synapses[28], $Hes5^+$ astrocytes could be a critical NA target for modulating pain in the SDH.

LC-NA neurons are known to respond to several external and internal stressors[29]. In rodent models of stress, nociceptive stimuli (e.g., electric shock, animal bite, etc.) are frequently employed as stressors. LC-NA neurons respond not only to stimuli that directly excite nociceptors[30,31], but also to stressors that do not involve their direct stimulation[30,32]. Several studies using rodent stress models have shown that exposure to stressors with or without nociceptor activation induces a remarkable change in pain-associated behavior[33,34]. Despite the

impact of stress on the pain system, the mechanism underlying a link between stress and pain, especially pain exacerbation, at the neural circuit and cellular levels remains poorly understood, although it has been proposed that activation of enkephalinergic and GABAergic INs in the SDH is involved in stress-induced pain inhibition[35]. Since stressful events are known to have a significant impact on chronic pain[36,37], providing new insights into the mechanisms by which stress modulates pain is also of clinical importance.

In this study, we investigated how stress modulates pain with a focus on $LC^{\rightarrow SDH}$-NA neurons and their target $Hes5^{+}$ astrocytes in the SDH, using multiple approaches. Our experiments using *in vivo* Ca^{2+} imaging, chemogenetics and optogenetics, cell ablation, electrophysiology, biochemical imaging for NA release and astrocytic Ca^{2+} responses, conditional gene knockout, and behavioral analyses demonstrate for the first time that $LC^{\rightarrow SDH}$-NA neuronal signaling to $Hes5^{+}$ SDH astrocytes and subsequent astrocytic reduction of SDH-IN activity are essential for stress-induced mechanical pain hypersensitivity.

Results

$LC^{\rightarrow SDH}$-NA neurons mediate mechanical hypersensitivity after acute restraint stress.

To investigate the mechanism underlying stress-induced pain modulation, we subjected wild-type (WT) mice to acute restraint stress exposure (Figure 1A), a well-known and frequently used stress model[29]. Consistent with a previous study[38], restraint stress for 30 min and 1 hour induced hypersensitivity to light mechanical stimuli (by applying von Frey filaments) to the plantar skin of the hindpaw (Figure 1B). However, with longer exposure (2 hours) to restraint stress, mechanical hypersensitivity was attenuated (Figure S1). In subsequent experiments, we chose 1 hour as the exposure time to restraint stress. To analyze LC-NA neuronal activity during restraint stress, we performed fiber photometry using *NET-Cre* mice (Cre is expressed in NAergic neurons under the control of the promoter of NA transporter [NET])[39] with microinjection into the LC of an adeno-associated viral (AAV) vector designed to express GCaMP6s (genetic encoded fluorescent Ca^{2+} indicator) in a Cre-dependent manner (AAV-flex[GCaMP6s]). Three weeks after the injection, GCaMP6s was expressed selectively in tyrosine hydroxylase^{+} (TH^{+}) LC-NA neurons (Figure 1C)[40]. We found that restraint stress exposure increased the number of Ca^{2+} events in these neurons (Figure 1, D and E; Figure S2). The number of Ca^{2+} events was highest during the first 20 min of the restraint stress exposure and gradually decreased later.

103 To investigate the role of LC-NA neurons in mechanical hypersensitivity, we utilized a cell
104 ablation approach[41]; diphtheria toxin (DTX) receptors (DTR) were specifically expressed in LC-
105 NA neurons by injection of AAV-flex[DTR-EGFP] into the LC of *NET-Cre* mice (Figure 1F).
106 DTR^+ neurons (detected by GFP) mainly co-expressed TH, and these neurons were ablated by
107 DTX administration (10 µg/kg, two injections 24-hour apart), which resulted in a loss of TH
108 signal in the LC and reduction of NET signal in the SDH (Figure 1G). We performed behavioral
109 tests in these mice and observed that ablation of LC-NA neurons abolished mechanical
110 hypersensitivity after restraint stress exposure (Figure 1H). To specifically ablate $LC^{\rightarrow SDH}$-NA
111 neurons, a retrograde AAV vector expressing Cre (AAVretro-Cre) was injected into the L4 SDH,
112 followed by AAV-flex[DTR-EGFP] injection into the LC (Figure 1I). In these mice, TH^+
113 $LC^{\rightarrow SDH}$-NA neurons expressing DTR (detected by EGFP) were ablated after DTX administration
114 (Figure 1J). These mice also failed to induce mechanical hypersensitivity after the restraint stress
115 (Figure 1K). These results suggest that descending $LC^{\rightarrow SDH}$-NA neurons are necessary for
116 mechanical pain hypersensitivity after acute restraint stress exposure. Furthermore, we tested
117 whether optogenetic activation of $LC^{\rightarrow SDH}$-NA neurons could induce mechanical hypersensitivity,
118 using ChrimsonR, a well-established red-shifted channelrhodopsin[42]. *NET-Cre* mice were
119 microinjected with AAV-flex[ChrimsonR-tdTomato] into the LC (Figure 1L). Three weeks later,
120 we confirmed expression of ChrimsonR (detected by tdTomato) in TH^+ neurons in the LC and
121 NET^+ axons/terminals in the SDH (Figure 1M). Optogenetic stimulation of $LC^{\rightarrow SDH}$-NA neuronal
122 axons/terminals in the SDH evoked mechanical hypersensitivity in these mice (Figure 1N). These
123 results together demonstrate that $LC^{\rightarrow SDH}$-NA neurons are activated by acute stress exposure and
124 are not only necessary for stress-induced mechanical pain hypersensitivity but also sufficient to
125 phenocopy the behavioral response.

126 **$LC^{\rightarrow SDH}$-NAergic signaling to $Hes5^+$ SDH astrocytes is required for stress-induced**
127 **mechanical hypersensitivity.**

128 To investigate the mechanism by which activation of $LC^{\rightarrow SDH}$-NA neurons induces mechanical
129 hypersensitivity, we first examined if NA is released in the SDH when these neurons are
130 stimulated, using the genetically encoded fluorescent NA sensor $GRAB_{NE1m}$[43]. In spinal cord
131 slices from *NET-Cre* mice that had been injected AAV-flex[ChrimsonR-tdTomato] into the LC
132 and AAV-gfaABC$_1$D-$GRAB_{NE1m}$ (expressing $GRAB_{NE1m}$ under the control of the astrocyte-
133 selective promoter gfaABC$_1$D[44] into the SDH) (Figure 2A), optogenetic stimulation of $LC^{\rightarrow SDH}$-
134 NA axons/terminals increased $GRAB_{NE1m}$ fluorescence intensity (Figure 2B), confirming NA
135 release from $LC^{\rightarrow SDH}$-NA neuron terminals in our slice conditions. The fluorescence intensity

136 increased in a stimulation period-dependent manner (Figure 2C). Next, to determine the target
137 cells and receptors of LC$^{\rightarrow SDH}$-NA neurons, we focused on α_{1A}Rs in astrocytes because our
138 previous study showed that NA increases $[Ca^{2+}]_i$ in astrocytes via α_{1A}Rs[22]. Using spinal cord
139 slices from *NET-Cre* mice that had been injected with AAV-flex[ChrimsonR-tdTomato] into the
140 LC and AAV-gfaABC$_1$D-GCaMP6m into the SDH (Figure 2A), we found that optogenetic
141 stimulation of LC$^{\rightarrow SDH}$-NA axons/terminals evoked a rise in $[Ca^{2+}]_i$ in astrocytes (Figure 2, D and
142 E). Pretreatment with the α_{1A}R-specific antagonist silodosin (40 nM) suppressed the Ca^{2+}
143 responses (Figure 2F), suggesting that NA released from LC$^{\rightarrow SDH}$-NA neurons induces Ca^{2+}
144 responses in SDH astrocytes via α_{1A}Rs. Behaviorally, intrathecal injection of silodosin in *NET-*
145 *Cre*;AAV-ChrimsonR mice attenuated mechanical hypersensitivity by optogenetic stimulation of
146 the LC$^{\rightarrow SDH}$-NA neurons (Figure 2G). Consistent with our previous findings[22], intrathecal
147 administration of NA (0.1 nmol) evoked transient mechanical hypersensitivity, which was
148 completely abolished in *Hes5-CreERT2*;*Adra1a*$^{flox/flox}$ mice treated with tamoxifen (Hes5$^+$
149 astrocyte-selective conditional knockout of α_{1A}Rs: Hes5$^+$ astrocyte–α_{1A}R cKO) (Figure 2H).
150 Moreover, mechanical hypersensitivity after acute restraint stress was abolished in Hes5$^+$
151 astrocyte–α_{1A}R cKO mice (Figure 2I). In addition, intrathecal administration of 5,7-
152 dichlorokynurenic acid (DCK; 10 nmol), an antagonist of D-serine signaling on N-methyl-D-
153 aspartate (NMDA) receptors, also suppressed mechanical hypersensitivity (Figure 2J). Supporting
154 this finding, our previous report identified D-serine as a hypersensitivity-inducing factor released
155 from Hes5$^+$ astrocytes[22]. These results indicate that spinally-released NA from LC$^{\rightarrow SDH}$-NA
156 neurons after acute restraint stress activates α_{1A}Rs on Hes5$^+$ astrocytes, which causes mechanical
157 pain hypersensitivity.

158 **Hes5$^+$ astrocytes mask IN function via adenosine A_1 receptors.**

159 Besides astrocytes, *Adra1a* mRNA is also expressed in INs in the SDH[13,14]. However, *Vgat-*
160 *Cre*;*Adra1a*$^{flox/flox}$ mice (Vgat$^+$ IN-selective conditional knockout of α_{1A}Rs: Vgat$^+$ IN–α_{1A}R cKO
161 mice)[14,16] had no effect on the NA (0.1 nmol)-induced mechanical hypersensitivity (Figure 3A). A
162 similar behavioral phenotype was also observed after intrathecal administration of phenylephrine
163 (0.05 nmol), a selective agonist for α_1Rs (Figure 3B). Furthermore, stress-induced mechanical
164 hypersensitivity was not affected in Vgat$^+$ IN–α_{1A}R cKO mice (Figure 3C). Considering previous
165 data that SDH-INs (including Vgat$^+$) respond to NA via α_{1A}Rs at NA concentrations similar to
166 those that elicit Hes5$^+$ astrocyte response[16,22], it remains unclear why intrathecally administered
167 NA and spinally released NA from LC$^{\rightarrow SDH}$-NA neuron terminals (after acute restraint stress)
168 have no suppressive effect via α_{1A}R-mediated Vgat$^+$ IN activation on mechanical hypersensitivity.

169 We then hypothesized an interaction between Hes5$^+$ astrocytes and Vgat$^+$ INs as per a previous
170 report that optogenetic activation of rat SDH astrocytes leads to ATP release; ATP is converted to
171 adenosine extracellularly which subsequently suppresses the activity of SDH-INs via adenosine
172 A_1 receptors (A_1Rs)[45]. By performing whole-cell current-clamp recordings of Vgat$^+$ INs in spinal
173 cord slices from *Vgat-Cre*;*Rosa-tdTomato* mice, we found that bath application of NA (20 μM)
174 evoked depolarization in 22.2% (10/45 cells) of tdTomato$^+$ cells (Vgat$^+$ INs), with 30% of these
175 showing action potentials (3/10 cells). The proportion of Vgat$^+$ INs depolarized by NA is similar
176 to that of *Adra1a* mRNA-expressing INs[14]. In 50% (5/10 cells) of depolarized Vgat$^+$ INs,
177 additional application of the A_1R-selective agonist N6-cyclopentyladenosine (CPA; 1 μM)
178 suppressed NA-induced depolarization/action potentials (Figure 3D and E). Supporting this
179 finding, RNAscope *in situ* hybridization detected *Adora1* mRNA fluorescence in 63.5 ± 6.9% of
180 *Slc32a1* (*Vgat*)$^+$ INs (n = 497, from three mice) (Figure 3F). Because A_1Rs are also expressed in
181 the dorsal root ganglion neurons[46], excitatory neurons and microglia[47] in the SDH, we employed
182 the CRISPR–Cas9 system using AAV vectors to specifically knockdown A_1Rs in SDH-INs.
183 AAV vectors designed to express the *Staphylococcus aureus* Cas9 (SaCas9)[48] in a Cre-dependent
184 manner (AAV-flex[SaCas9]) and single guide RNA-expression vectors (AAV-flex[mCherry]-
185 U6-sgAdora1 or -flex[mCherry]-U6-sgYFP [as a control]) were co-microinjected into the SDH of
186 *Vgat-Cre* mice (Figure 3G). SaCas9 (detected by HA-tag) and mCherry-labeled cells in the SDH
187 were immunolabeled with paired box 2 (PAX2) (Figure 3G), a marker of INs[49]. In these SDH-
188 Vgat$^+$ IN-selective A_1R conditional knockdown mice (SDH-Vgat$^+$ IN–A_1R cKD mice), the
189 inhibitory effect of CPA on NA-induced depolarization/action potentials was completely
190 abolished in mCherry$^+$ neurons (Figure 3, H and I). Using a chemogenetic approach with
191 modified human muscarinic G_q-protein-coupled receptors (hM3Dq)[50], we further examined the
192 effect of G_q-stimulated Hes5$^+$ astrocytes on inhibitory synaptic transmission. *Hes5-CreERT2* mice
193 were microinjected with AAV-flex[hM3Dq-HA] into the SDH (*Hes5-CreERT2*;AAV-hM3Dq
194 mice). hM3Dq (detected by HA-tag) was expressed in the SDH, and these cells were double-
195 labeled with glial fibrillary acidic protein (GFAP) and SRY-related high-mobility group box 9
196 (SOX9), markers of astrocytes (Figure 3J). Using spinal cord slices from these mice, we
197 performed whole-cell voltage-clamp recordings of substantia gelatinosa (SG) neurons. Bath
198 application of hM3Dq agonist clozapine N-oxide (CNO; 100 μM) reduced the frequency of
199 spontaneous inhibitory postsynaptic currents (sIPSCs) in SG neurons (Figure 3, K and L). This
200 effect was prevented by pretreatment with the A_1R-specific antagonist, 8-cyclopentyl-1,3-
201 dimethylxanthine (CPT; 1 μM) (Figure 3, M and N). These results suggest that a signaling
202 pathway from Hes5$^+$ astrocytes suppresses the activity of Vgat$^+$ INs via A_1Rs in the SDH.

203 **Hes5$^+$ astrocyte-mediated inhibitory signals to INs affect mechanical hypersensitivity.**

204 We investigated whether A_1Rs in SDH-Vgat$^+$ INs contributed to the mechanical hypersensitivity
205 elicited by intrathecal NA (0.1 nmol). Acute inhibition of spinal A_1Rs by intrathecal
206 administration of CPT (3 nmol) suppressed NA-induced mechanical hypersensitivity (Figure 4A).
207 Similarly, SDH-Vgat$^+$ IN–A_1R cKD mice showed a significant reduction in the behavioral
208 hypersensitivity by NA (Figure 4B), indicating that A_1Rs in SDH-Vgat$^+$ INs contribute to
209 mechanical hypersensitivity by spinal NA. Furthermore, SDH-Vgat$^+$ IN–A_1R cKD mice and
210 intrathecal-CPT-pretreated mice exhibited a significant attenuation of the stress-induced
211 mechanical hypersensitivity (Figure 4, C and D). These results suggest that Hes5$^+$ astrocyte-
212 mediated negative control for SDH-Vgat$^+$ INs via A_1R-mediated signals is crucial for stress-
213 induced mechanical hypersensitivity. Moreover, we investigated the role of this interaction in
214 stress-induced alteration of somatosensory information processing in the SDH using
215 phosphorylated extracellular signal-regulated kinase (pERK), a neuronal nociceptive input marker
216 in superficial SDH neurons[51]. Consistent with the results of a previous report[52], Aβ fiber
217 stimulation of the hindpaw alone did not increase the number of pERK$^+$ neurons in the superficial
218 SDH (laminae I–IIi using isolectin B4 [IB4], a marker of lamina IIi) (Figure 4, E and F).
219 Similarly, acute restraint stress alone did not change the number of pERK$^+$ neurons (Figure 4, E
220 and F). Interestingly, Aβ fiber stimulation following acute restraint stress exposure significantly
221 increased the number of pERK$^+$ neurons in the superficial SDH (Figure 4, E and F). Intrathecal
222 injection of CPT prevented the stress-induced increase in pERK$^+$ neurons (Figure 4, E and F).
223 These results suggest that the abnormal responsiveness of superficial SDH neurons to signals
224 from Aβ fibers in mice with acute restraint stress, involves adenosine signals that are important
225 for negatively controlling Vgat$^+$ INs by NA-stimulated Hes5$^+$ astrocytes and for mechanical
226 hypersensitivity.

227

228 **Discussion**

229 External and internal stressors elicit a variety of biological responses including pain modulation.
230 Acute exposure to a stressor inhibits or facilitates behavioral responses to thermal and mechanical
231 stimuli applied to the skin[33,38,53]. While the mechanism underlying pain inhibition has been
232 studied[33], the neural basis of pain facilitation by stress remains poorly understood. In this study,
233 we identified a circuit, the descending LC$^{\rightarrow SDH}$-NA neurons, that is activated by acute restraint
234 stress exposure and demonstrated that the circuit is necessary for stress-induced pain

235 hypersensitivity. A notable finding of this study was that Hes5$^+$ astrocytes, a subpopulation of
236 spinal cord astrocytes[22], are the primary target of NA released from descending LC$^{\rightarrow SDH}$-NA
237 neurons for mechanical pain hypersensitivity caused by stress. Thus, this top-down signaling
238 pathway from LC$^{\rightarrow SDH}$-NA neurons to Hes5$^+$ SDH astrocytes is an essential link between stress
239 and pain sensitization.

240 Spinal NA derived from LC-NA neurons has been classically implicated in pain inhibitory
241 control[9-11]. The suggested mechanism to this effect is its action on SDH-INs via α_{1A}Rs[9,16]. In
242 contrast, recent our study has unveiled another facet of spinal NA signaling, which is
243 pronociceptive, by identifying Hes5$^+$ astrocytes in the SDH[22]. Mechanistically, spinal NA acts on
244 α_{1A}Rs expressed on Hes5$^+$ astrocytes, increases intracellular Ca^{2+} levels via a G_q/PLC/IP_3
245 pathway, and causes mechanical hypersensitivity via release of D-serine[22], an activator of NMDA
246 receptors. This study showed that the optogenetic activation of LC$^{\rightarrow SDH}$-NA neurons produced
247 mechanical hypersensitivity via α_{1A}Rs in SDH-Hes5$^+$ astrocytes, indicating the pronociceptive
248 effect of LC$^{\rightarrow SDH}$-NAergic signaling. In contrast, it has also been reported that a similar opto- or
249 chemogenetic activation produces an antinociceptive effect on thermal stimuli[54,55]. The reason for
250 the difference remains unclear; however, the stimulus modality used for the behavioral assay
251 (mechanical vs. thermal) may be responsible, since the SDH circuits for mechanical and thermal
252 information processing have been shown to be distinct[3,56-59].

253 Given that SDH-INs also express α_{1A}Rs[13,14], it is unclear why pain hypersensitivity is the
254 preferentially manifested behavioral phenotype after activation of LC$^{\rightarrow SDH}$-NAergic signal. This
255 study showed that NA-stimulated Hes5$^+$ astrocytes negatively regulate the activity of SDH-Vgat$^+$
256 INs. This astrocytic attenuation of SDH-Vgat$^+$ IN activity may involve adenosine signaling
257 because A_1R cKD in SDH-Vgat$^+$ INs canceled the suppressive effect of A_1R agonist on NA-
258 induced enhancement of Vgat$^+$-IN activity and NA-induced mechanical hypersensitivity. The
259 adenosine-mediated inhibition of SDH-INs is consistent with the data from a previous study[45].
260 Thus, these results suggest that spinal NA acts on α_{1A}Rs expressed by both Hes5$^+$ astrocytes and
261 Vgat$^+$ INs; however, NA-stimulated Hes5$^+$ astrocytes suppress Vgat$^+$ IN activity by adenosine
262 signaling via A_1Rs; this induces a state where the Hes5$^+$ astrocyte-derived pain-facilitating effect
263 predominates, causing mechanical pain hypersensitivity (Figure 4G).

264 While a neuronal model for gating peripherally derived sensory signals in the SDH has been
265 previously established by identifying several subpopulations of INs[1-5], our study proposes a new
266 regulatory mechanism in this model in which Hes5$^+$ astrocytes act as non-neuronal gating cells in

267 the SDH for brain-derived NAergic signaling. This astrocytic gating control of INs may affect
268 processing and transmission of somatosensory information in the SDH. Indeed, a
269 pharmacological blockade of the adenosine signal to SDH-Vgat$^+$ INs suppressed the Aβ fiber-
270 mediated pERK expression in the superficial SDH of stressed mice. Preproenkephalin$^+$ IN
271 population may be among the SDH-Vgat$^+$ INs involved in stress-induced pain modulation[35].
272 Interfering with GABA/glycine signaling in the SDH results in abnormal synaptic inputs from
273 primary afferent Aβ fibers onto superficial SDH neurons[60]. Our view is also supported by
274 previous findings from *in vivo* patch-clamp recordings, which show that, in about a half of SG
275 neurons tested, NA enhances excitatory synaptic responses evoked by tactile stimuli (air puff to
276 the skin)[61]. Additionally, our hypothesis that Hes5$^+$ astrocytes co-release D-serine and
277 ATP/adenosine in response to α_{1A}R activation by NA is supported by previous findings in the
278 neocortex[62]. Aβ fiber inputs into neurokinin 1 receptor-positive projection neurons in SDH
279 lamina I following inhibition of GABA/glycine signaling is canceled by a pharmacological
280 blockade of NMDA receptors[60], supporting our data that the stress-induced mechanical
281 hypersensitivity was suppressed by the antagonist of D-serine site of NMDA receptors DCK.
282 However, the effect of astrocytic adenosine on spinal pain processing has been controversial:
283 both, pronociceptive (consistent with our findings)[45] and antinociceptive[63]. Such different effects
284 might be related in part to the regionally restricted astrocytic subpopulations and factors for their
285 activation. Pro- and anti-nociceptive effects have been reported to be mediated by astrocytes
286 located in superficial and deeper laminae and stimulated by NA (via G protein-coupled α_{1A}Rs)[22]
287 and ATP (via ionotropic P2X7 receptors)[63], respectively. In particular, the regional differences in
288 the role of astrocytes has been demonstrated by our previous study in which a selective
289 chemogenetic stimulation of astrocytes in deeper SDH did not cause mechanical
290 hypersensitivity[22]. Thus, it is conceivable that locally released adenosine from NA-stimulated
291 Hes5$^+$ astrocytes, following acute restraint stress, may suppress SDH-Vgat$^+$ IN function, which
292 results in mechanical pain hypersensitivity. The spatially restricted neuron–astrocyte
293 communication needs to be investigated in future studies.

294 In this study, we focused on the mechanisms of mechanical hypersensitivity by acute exposure to
295 restraint stress. Consistent with a recent study[38], acute restraint stress caused mechanical
296 hypersensitivity; however, there are also reports showing a reduction in behavioral responses to
297 thermal or mechanical stimuli upon exposure to similar restraint stress[33,35]. A precise explanation
298 for the bidirectional outcomes remains elusive. However, it is widely recognized that the extent
299 and direction of pain modulation may be due to the nature, duration, and intensity of the

300 stressor[33,34]. Indeed, while acute and short-term exposure (≤1 hour) to restraint stress induces
301 mechanical pain hypersensitivity, longer exposure (2 hours) failed to exhibit the behavioral
302 response (Figure S1). It has also been reported that behavioral response to nociceptive thermal
303 stimuli is suppressed by a 2-hour exposure to restraint stress[16]. Thus, descending $LC^{\rightarrow SDH}$-NA
304 neurons, $Hes5^{+}$ SDH astrocytes, or their output signals may be attenuated by unidentified
305 inhibitory signals evoked by longer exposure to restraint stress. In addition, a similar bidirectional
306 behavioral outcome on mechanical pain has also been observed with intrathecal NA; low doses of
307 NA induce mechanical pain hypersensitivity while higher doses do not[22]. Thus, the bidirectional
308 change may depend on the level of NA neuronal activity and NA content in the SDH, which is
309 supported by a previous report[64].

310 Clinically, stressor-evoked psychological and physical responses are considered critical for the
311 development of chronic pain[36], especially nociplastic pain, a condition that arises from altered
312 nociceptive signaling without actual or threatened tissue damage, or disease or lesion of the
313 somatosensory system[37]. In fact, patients with chronic pain have a high incidence of stress-related
314 psychiatric disorders, such as anxiety, fear, and depression[11,65]; stressful life events are known to
315 be a key factor in establishing fibromyalgia and enhance pain in patients with irritable bowel
316 syndrome and headaches[37]. Thus, our findings provide a mechanistic insight into the link between
317 stress and pain modulation and may help in understanding and developing a new strategy for
318 chronic pain, including nociplastic pain.

319

Methods

Animals: Male C57BL/6J mice (CLEA Japan), male and female *NET-Cre* mice [Tg(*Slc6a2-cre*)#Stl] (kindly provided by Prof. Thomas McHugh, RIKEN Center for Brain Science)[39], *Hes5-CreERT2* mice [Tg(*Hes5-cre/ERT2*)^{2Vtlr}] (kindly provided by Prof. Verdon Taylor)[66], *Adra1a*$^{flox/flox}$ mice[22], *Vgat-Ires-Cre* mice [*Slc32a1*$^{tm2(cre)Lowl}$/J] (Stock No: 016962, The Jackson Laboratory)[67], and *Rosa26-tdTomato* mice [B6.Cg-*Gt(ROSA)26Sor*$^{tm14(CAG-tdTomato)Hze}$/J] (Stock No: 007914, The Jackson Laboratory)[68] were used. To generate *Hes5-CreERT2*;*Adra1a*$^{flox/flox}$ mice[22] or *Vgat-Cre*;*Adra1a*$^{flox/flox}$ mice[16], *Adra1a*$^{flox/flox}$ mice were crossed with *Hes5-CreERT2* mice or *Vgat-Ires-Cre* (*Vgat-Cre*) mice, and the obtained *Hes5-CreERT2*;*Adra1a*$^{flox/+}$ mice or *Vgat-Cre*;*Adra1a*$^{flox/+}$ mice were further crossed with *Adra1a*$^{flox/flox}$ mice. Cre-negative *Adra1a*$^{flox/flox}$ littermate mice were used as controls. For induction of CreERT2 recombinase activity, *Hes5-CreERT2* mice were given an intraperitoneal (i.p.) injection of tamoxifen (#T5648, Sigma-Aldrich; 2 mg dissolved in 100 μl corn oil [#032-17016; Wako, Saitama, Japan]) once a day for 5–10 successive days. We used tamoxifen-injected mice for further analyses 7 days or more after the last injection. All mice used were 8–12 weeks of age at the start of each experiment and were housed at temperature and humidity ranges of 21–23°C and 40–60%, respectively, with a 12-hour light-dark cycle. All animals were fed food and water ad libitum. All animals were housed in standard polycarbonate cages in groups of same-sex littermates. All animal experiments were conducted according to relevant national and international guidelines contained in the 'Act on Welfare and Management of Animals' (Ministry of Environment of Japan) and 'Regulation of Laboratory Animals' (Kyushu University) and under the protocols approved by the Institutional Animal Care and Use committee review panels at Kyushu University.

Restraint stress model: According to the methods described in our previous study[16], mice were restrained by placing them in a Falcon® 50-ml conical tube (#352070; Corning) with a hole in the tip. The space remaining behind the mouse was filled with a paper towel. Mice were allowed to breathe but not turn around. Control mice were handled briefly and placed in home cages without water or food for 1 hour.

Measurement of behavioral response to mechanical stimuli using von Frey filaments: Mice were placed individually in an opaque plastic cylinder, which was placed on a wire mesh, and habituated for 0.5–1 hour to allow acclimatization to the new environment. After that, calibrated von Frey filaments (0.02–2.0 g; #NC12775; North Coast Medical) were applied to the plantar surface of the hindpaw of mice from below the mesh floor. 50% paw withdrawal threshold was

352 calculated using the up-down method[69]. The basal mechanical threshold was determined by
353 performing von Frey test before restraint stress exposure, AAV microinjection, DTX
354 administration, optogenetic stimulation, intrathecal injection of several drugs and tamoxifen
355 administration. Mechanical sensitivity was evaluated at 30, 60, 90, 120 and 180 min after restraint
356 stress or optogenetic stimulation, or at 30 min after intrathecal injection of NA or Phe.

357 **Recombinant AAV (rAAV) vector production:** pAAV-CAG-flex[GCaMP6s]-WPRE
358 (#100842) and pAAV-synapsin (Syn)-flex[ChrimsonR-tdTomato]-WPRE (#62723) were
359 purchased from Addgene. The genes encoding GCaMP6m (#40754; Addgene), Cre, and
360 $GRAB_{NE1m}$ (#123308; Addgene) were subcloned into the pENTR plasmid (Thermo Fisher
361 Scientific). To produce AAV vectors, we inserted GCaMP6m and $GRAB_{NE1m}$ into pZac2.1-
362 gfaABC$_1$D-WPRE plasmid and Cre into pZac2.1-enhanced synapsin (ESYN)-WPRE plasmid. To
363 produce the AAV vector for the Cre-switch system, vectors containing the promoters encoding
364 EF1α were generated from pAAV-CA-FLEX (#38042; Addgene) by substituting the promoter.
365 We then inserted AcGFP, DTR-EGFP (kindly provided by Prof. Kenji Kohno, Nara Institute of
366 Science and Technology), mCherry and hM3Dq (#45547; Addgene) into pAAV-EF1α-FLEX.
367 The genes encoding U6-sgRNA (#61593; Addgene) and SaCas9 (#78601; Addgene) were
368 subcloned into the pENTR plasmid. Synthetic oligonucleotides including the targeting sequence
369 for *Adora1* (5'-AAGTTCCGGGTCACCTTTCTG-3') and non-targeting sequence (5'-
370 CCATGTGATCGCGCTTCTCGT-3') were replaced with the targeting site in the original
371 pENTR-U6-sgBsa1 plasmid. The resulting U6-sgRNA cassette was transferred into pAAV-
372 CMV-flex[mCherry]-WPRE plasmid to generate pAAV-CMV-flex[mCherry]-WPRE-U6-
373 sgAdora1/sgYFP (sgControl). The SaCas9 cassette was transferred into pAAV-CMV-flex-WPRE
374 plasmid to generate pAAV-CMV-flex[SaCas9]-WPRE. rAAV vectors were produced from
375 human embryonic kidney 293T (HEK293T) cells with triple transfection [pZac or pAAV, cis
376 plasmid; pAAV2/5 (University of Pennsylvania Gene Therapy Program Vector Core), pAAV2/9
377 (University of Pennsylvania Gene Therapy Program Vector Core) or pAAV2/retro (#81070;
378 Addgene), trans plasmid; pAd DeltaF6, adenoviral helper plasmid (University of Pennsylvania
379 Gene Therapy Program Vector Core)] and purified by two cesium chloride density gradient
380 purification steps. The vector was dialyzed against phosphate-buffered saline (PBS) containing
381 0.001% (v/v) Pluronic-F68 (#24040032; Thermo Fisher Scientific) using Vivaspin Turbo 15
382 100,000 MWCO (#VS15T41; Sartorius). The genome titer of rAAV was determined by Pico
383 Green fluorometric reagent (#P7589; Thermo Fisher Scientific) following denaturation of the
384 AAV particles. Vector were stored at −80°C until use.

385 **Intra-SDH and intra-LC injection of rAAV vectors:** Viral injection was performed in
386 accordance with our previously described method[22,70]. Mice were deeply anesthetized by
387 subcutaneous injection of ketamine (100 mg/kg) and xylazine (10 mg/kg). For intra-SDH
388 injection, the skin was incised at Th11–L4 vertebrae, and custom-made clamps were attached to
389 the caudal sites of the vertebral column. Paraspinal muscles around the left side of the interspace
390 between Th13 and L1 vertebrae were removed, and the dura mater and arachnoid membrane were
391 carefully incised using the tip of a 30-G needle to make a small window allowing a glass
392 microcapillary to insert directly into the SDH. The microcapillary was inserted into the unilateral
393 SDH (around 120–150 μm in depth from the surface of the dorsal root entry zone). rAAV
394 solutions (approximately 500 nl) were injected using a Micro4 Micro Syringe Pump Controller
395 (World Precision Instrument). After microinjection, the glass microcapillary was removed, the
396 skin was sutured with 5-0 silk, and the mice were kept on a heating pad until recovery. For intra-
397 LC injection, rAAV solutions were injected (approximately 300 nl in one site) adjacent to the LC
398 (anteroposterior (AP): −5.4 mm from the bregma; mediolateral (ML): ±0.9 mm; dorsoventral
399 (DV): −3.2 mm from the dura). Only AAV2/9-CAG-flex[GCaMP6s]-WPRE was injected
400 unilaterally, and the other AAV vectors were injected bilaterally. To keep the bregma and lambda
401 in the same horizontal plane, tolerance was maintained at <50 μm in the dorsoventral axis
402 between the bregma/lambda. The microcapillary was withdrawn 3 min after ending the injection.
403 The skin was then sutured with 5-0 silk, and the mice were kept on a heating pad until recovery.
404 We used virus-injected mice for further analyses 3 weeks or more after the last injection. The
405 following viral titers were used: AAV2/9-CAG-flex[GCaMP6s]-WPRE, AAV2/9-gfaABC$_1$D-
406 GCaMP6m-WPRE, AAV2/9-EF1α-flex[AcGFP]-WPRE (for *NET-Cre* mice), AAV2/9-EF1α-
407 flex[DTR-EGFP]-WPRE (for *NET-Cre* mice), AAV2/9-EF1α-flex[mCherry], AAV2/9-hSyn-
408 flex[ChrimsonR-tdTomato], AAV2/9-gfaABC$_1$D-GRAB$_{NE1m}$-WPRE, AAV2/5-EF1α-
409 flex[hM3Dq] and AAV2/9-CMV-flex[SaCas9]-WPRE: 1.0×10^{12} genome copies (GC)/ml;
410 AAV2/retro-ESYN-Cre-WPRE: 3.0×10^{12} GC/ml; AAV2/9-EF1α-flex[AcGFP] (for WT mice)
411 and AAV2/9-EF1α-flex[DTR-EGFP]-WPRE (for WT mice): 2.0×10^{12} GC/ml; AAV2/9-CMV-
412 flex[mcherry]-WPRE-U6-sgYFP and AAV2/9-CMV-flex[mcherry]-WPRE-U6-sgAdora1: $0.5 \times$
413 10^{12} GC/ml.

414 **Immunohistochemistry:** Mice were deeply anesthetized with an i.p. injection of pentobarbital
415 and transcardially perfused with PBS (#041-20211; Wako, Saitama, Japan) followed by ice-cold
416 4% paraformaldehyde (PFA; #162-16065; Wako, Saitama, Japan)/PBS. The transverse L4
417 segments of the spinal cord and brain were removed, postfixed in the same fixative for 3 hours

418 (spinal cord) or overnight (brain) at 4°C, and placed in 30% sucrose solution for 24–48 hours at
419 4°C. After incubation, the tissues were embedded in OCT compound (#4583; Sakura Finetek
420 Japan, Osaka, Japan) and stored at −25°C before use. Transverse spinal cord and brain sections
421 (30 μm) were incubated in blocking solution (3% normal goat serum [#S-1000; Vector
422 Laboratories] or normal donkey serum [#017-000-121; Jackson ImmunoResearch]) for 2 hours at
423 room temperature and then incubated for 48 hours at 4°C with primary antibodies: polyclonal
424 rabbit anti-tyrosine hydroxylase (TH; 1:1000; #AB152; Millipore); polyclonal sheep anti-TH
425 (1:1000; #AB1542; Millipore); monoclonal mouse anti-noradrenaline transporter (NET; 1:2000;
426 #NET05-2; Mab Technologies); polyclonal rabbit anti-green fluorescent protein (GFP; 1:1000;
427 #598; MBL International); monoclonal rabbit anti-hemagglutinin (HA)-tag (1:1000; #3724; Cell
428 Signaling); monoclonal rat anti-glial fibrillary acidic protein (GFAP; 1:2000; #13-0300;
429 Invitrogen); polyclonal goat anti-SRY-related high-mobility group box 9 (SOX9; 1:1000; #
430 AF3075; R&D Systems); polyclonal goat anti-paired box 2 (PAX2; 1:500; # AF3364; R&D
431 Systems); monoclonal rat anti-mCherry (1:2000; #M11217; Thermo Fisher Scientific); polyclonal
432 rabbit anti-phospho-p44/42 MAPK (ERK1/2) (Thr202/Tyr204) (pERK; 1:500; #9101; Cell
433 Signaling); anti-isolectin B4 (IB4)-biotin conjugate (1:1000; # I21414; Thermo Fisher Scientific).
434 After incubation, tissue sections were washed and incubated for 3 h at room temperature with
435 secondary antibodies (Alexa Fluor™ 488, 546 and/or 555; #A11001, A11008, A11035, A11056,
436 A11081, S32351; Thermo Fisher Scientific: #ab150178; Abcam: DyLight™ 405; #705-475-147;
437 Jackson ImmunoResearch). Then, tissue sections were washed, slide mounted, and subsequently
438 placed under coverslips with VECTASHIELD Hardmount (Vector Laboratories).
439 Immunofluorescence images were obtained with confocal laser microscopy (#LSM700; Carl
440 Zeiss).

441 **Fiber photometry:** Immediately after microinjection of AAV vectors encoding GCaMPs, the
442 mice were implanted with an optic cannula. Cannulae were purchased from RWD (#R-FOC-
443 BL400C-50NA, ø1.25 mm ferrule, ø400 μm optic fiber, 0.50 NA). The length of the optic fiber
444 protruding from the tip of the ferrule was 4.0 mm. Optic cannula was implanted in the unilateral
445 LC (AP: −5.4 mm from the bregma; ML: 0.9 mm; DV: −3.0 mm from the dura). Next, the
446 cannula was secured using two types of dental glues (Super-bond; Sun Medical, Shiga, Japan:
447 UNIFAST III; GC, Tokyo, Japan). After implantation, the skin was sutured with 5-0 silk, and the
448 mice were kept on a heating pad until recovery. We used cannula-implanted mice for fiber
449 photometry 3 weeks or more after the surgery. GCaMP fluorescent signals were obtained with the
450 fiber photometry apparatus from Doric Lenses, which includes a fiber photometry console

451 (FPC_V6), a 415-nm LED illumination (CLED_415), a 465-nm LED illumination (CLED_465),
452 an LED driver (LEDD_2), and a fluorescence mini cube with built-in fluorescence photodetector
453 amplifier (iFMC4-G2_IE(410-420)_E(460–490)_F(500–550)_S). A 415-nm light was modulated
454 at 208 Hz, while a 465-nm light was modulated at 572 Hz. The optic cannula implanted in mice
455 and fluorescence mini cube were connected by a low-autofluorescence patch cable (#MAF1L1;
456 Thorlabs). The power output at the fiber tip was 30–40 μW. After connecting to the patch cable,
457 the mice were allowed to move freely in the home cage for at least 10 min for habituation. After
458 habituation, fluorescence recording was started. Emitted signals from the tissue were collected
459 through the same fiber and sampled at 12 kHz.

460 **Processing and analysis of fiber photometry data:** To avoid the effects of photobleaching, data
461 from the first 5 min of recording were discarded. The raw data were then decimated to 30 Hz
462 (down-sampled by 400) and low-pass Butterworth-filtered at 2 Hz. The 415-nm excitation
463 channel served as an isosbestic, Ca^{2+}-independent control wavelength for GCaMP, allowing for
464 bleaching and movement artifact corrections when directly fitted to the Ca^{2+}-dependent 465-nm
465 channel. The Correction Baseline function from Doric Neuroscience Studio (Doric Lenses) was
466 used to fit the 415-nm signal to the 465-nm signal using an adaptive iterative re-weighted
467 Penalized Least Squares algorithm[71]. The fluorescence change was expressed as a relative
468 change, $\Delta F/F = (F_{465}-F_{415})/F_{415}$, where F_{465} is the 465 nm-induced Ca^{2+}-dependent signal, and
469 F_{415} is the 415 nm-induced Ca^{2+}-independent signal. Robust Z-scores were then calculated as Z =
470 ($\Delta F/F$−Median $\Delta F/F$)/NIQR, where Median $\Delta F/F$ is the median of $\Delta F/F$ during the entire
471 measurement period, and NIQR is the normalized interquartile range (0.7413 × interquartile
472 range). Ca^{2+} events were detected with a threshold of Z-score >3. The frequency of Ca^{2+} events
473 was calculated as the number of Ca^{2+} events per minute in the 10 min before stress, 60 min during
474 stress (10 min × 6 times), and 10 min after stress.

475 **Drug administration:** To ablate DTR^+ neurons, DTX (10 μg/kg in PBS; #048-34371; Wako,
476 Saitama, Japan) was administered i.p. for two successive days 3 weeks after intra-LC injection of
477 AAV2/9-EF1α-flex[DTR-EGFP] or [AcGFP]-WPRE. We used DTX-injected mice for further
478 analyses 2 weeks or more after the last injection. For intrathecal injection, a 30-G needle attached
479 to a Hamilton microsyringe was inserted between the L5/L6 vertebrae and then punctured
480 through the dura. The following drugs and doses were used for intrathecal injection experiments:
481 silodosin (3 nmol in 5 μl PBS; #191-17591; Wako, Saitama, Japan; injection was given 30 min
482 before optogenetic stimulation); L-norepinephrine hydrochloride (0.1 nmol in 5 μl saline;
483 #74480; Sigma-Aldrich); 5,7-dichlorokynurenic acid (DCK; 10 nmol in 5 μl saline of 2%

484 dimethylsulfoxide (DMSO); #0286; Tocris; injection was given immediately before the start of
485 exposure to restraint stress); (R)-(-)-phenylephrine hydrochloride (Phe; 0.05 nmol in 5 µl saline;
486 #163-11791; Wako, Saitama, Japan); 8-cyclopentyl-1,3-dimethylxanthine (CPT; 3 nmol in 5 µl
487 saline of 2% DMSO; #C102; Sigma-Aldrich; injection was given immediately before the start of
488 exposure to restraint stress or 30 min before intrathecal injection of NA).

489 ***In vivo* optogenetic stimulation:** Immediately after microinjection of AAV vectors encoding
490 ChrimsonR, mice were implanted with an optic cannula. A cannula comprised a ceramic ferrule
491 (#CFLC230-10; Thorlabs; ø1.25 mm, 6.4 mm length) and an optic fiber (#FT200UMT; Thorlabs;
492 ø200 µm, 0.39 NA). The length of the optic fiber protruding from the tip of the ferrule was less
493 than 0.3 mm. The vertebrae were immobilized in place using a metal bar along the Th12–L1. A
494 small laminectomy was performed through the Th13 bone using a dental drill. The cannula was
495 secured above the dura mater using two types of dental glues (Super-bond; Sun Medical:
496 UNIFAST III; GC). In this procedure, the dura mater and spinal cord parenchyma were left intact
497 and unscathed. After implantation, the skin was sutured with 5-0 silk, and the mice were kept on a
498 heating pad until recovery. We used cannula-implanted mice for optogenetic stimulation 3 weeks
499 or more after the surgery. To activate ChrimsonR in $LC^{\rightarrow SDH}$-NA axons/terminals, 625-nm LED
500 light (#M625F2; Thorlabs) was delivered through a ferrule patch cable (#M83L01; Thorlabs).
501 Light stimulations (2 mW, 10 Hz, 5-ms pulse duration, 5-s light on, 15-s light off, 10 cycles) were
502 generated by an LED driver (#LEDD_2; Doric Lenses).

503 **Fluorescent Ca^{2+} and NA imaging in spinal cord slices:** Fluorescent imaging was performed in
504 accordance with our previously described method[22]. GCaMP6m- and $GRAB_{NE1m}$-expressing mice
505 were anesthetized with an i.p. injection of urethane (1.2–1.5 mg/kg), and lumbosacral
506 laminectomy was performed. The spinal cord (L1–S2) was removed and placed in a cold, high-
507 sucrose, artificial cerebrospinal (aCSF) fluid (27 mM $NaHCO_3$, 1.4 mM NaH_2PO_4, 2.5 mM KCl,
508 7.0 mM $MgSO_4$, 1.0 mM $CaCl_2$, 222 mM sucrose, and 0.5 mM ascorbic acid), which was bubbled
509 with 95% O_2 and 5% CO_2. After cutting all ventral and dorsal roots, transverse L4 spinal cord
510 slices (350 µm thick) were made using a vibrating microtome (#VT1200; Leica); the slices were
511 kept in oxygenated aCSF solution (125 mM NaCl, 1.25 mM NaH_2PO_4, 2.5 mM KCl, 1.0 mM
512 $MgCl_2$, 2.0 mM $CaCl_2$, 26 mM $NaHCO_3$, and 20 mM glucose) at room temperature (22–25°C) for
513 at least 30 min before use. The slices were placed in a recording chamber, and fluorescent signals
514 were measured using a confocal laser scanning microscope (#FV3000; Olympus, Tokyo, Japan).
515 The chamber was perfused with aCSF saturated with 95% O_2 and 5% CO_2 at 31–32°C and at 2–3
516 ml/min using peristaltic pumps. A 488-nm diode laser was used for the excitation of GCaMP6m

517 and $GRAB_{NE1m}$. The size of the image was 509 × 509 μm^2 (512 × 512 pixels). The recordings
518 were acquired at a rate of 1.083 s per image. Light stimulations (1 mW, 10 Hz, 5-ms pulse
519 duration, 1–20 s) were generated by an LED driver (#LEDD_2; Doric Lenses) and delivered
520 through an optic fiber (Thorlabs, FT200UMT, ø200 μm, 0.39 NA). For an experiment on $\alpha_{1A}R$
521 inhibition, optogenetic stimulations (10 s) were performed twice (at least 15-min apart) in the
522 same slice. Silodosin (40 nM in aCSF) was continuously applied by bath application starting 5
523 min before the onset of 2nd optogenetic stimulation. After optogenetic stimulation, NA (1 or 10
524 μM in aCSF) was applied by bath application as the positive control.

525 **Processing and analysis of Ca^{2+} and NA imaging data:** Videos were imported into ImageJ Fiji
526 (https://imagej.net/software/fiji/), and motion artifacts were corrected using TurboReg[72]. The
527 fluorescence change was expressed as a relative percentage change, $\Delta F/F = 100 \times (F_t - F_0)/F_0$,
528 where F_t is the fluorescence at time t, and F_0 is the baseline average for 30 frames before the start
529 of stimulation. For Ca^{2+} imaging using GCaMP, the size of each region of interest (ROI) was set
530 to a circle with a diameter of 10 μm[22]. ROIs were manually identified based on the following
531 criteria: located within 200 μm from the surface of gray matter and ≥30% $\Delta F/F$ fluorescence
532 change after optogenetic stimulation or NA application. For the experiment on $\alpha_{1A}R$ inhibition,
533 normalized $\Delta F/F$ was calculated as ($\Delta F/F$ in 2nd stimulation)/($\Delta F/F$ in 1st stimulation). For NA
534 imaging using $GRAB_{NE1m}$, the raw image was binarized, and a single ROI was detected from such
535 a binarized image with the following parameters: contiguous pixel number >100 and
536 0 < circularity < 1[64]. Calculation of $\Delta F/F$ in ROIs was performed using the Time Series Analyzer
537 V3 plugin in ImageJ.

538 **Whole-cell patch-clamp recordings using spinal cord slices:** According to our previously
539 described method[16], mice were deeply anesthetized with urethane (1.2–1.5 mg/kg, i.p.), and the
540 lumbar spinal cord was removed and placed in a cold high-sucrose aCSF (250 mM sucrose, 2.5
541 mM KCl, 2 mM $CaCl_2$, 2 mM $MgCl_2$, 1.2 mM NaH_2PO_4, 25 mM $NaHCO_3$, and 11 mM glucose).
542 Parasagittal and transverse spinal cord slices (250–300 μm thick) were made with a vibrating
543 microtome (VT1200, Leica) and then the slices kept in oxygenated aCSF solution (125 mM
544 NaCl, 2.5 mM KCl, 2 mM $CaCl_2$, 1 mM $MgCl_2$, 1.25 mM NaH_2PO_4, 26 mM $NaHCO_3$, and 20
545 mM glucose) at room temperature (22–25°C) for at least 30 min. The spinal cord slice was then
546 put into a recording chamber, where it was continuously superfused with aCSF solution at 25–
547 28°C at a flow rate of 4–6 ml/min. Recordings were made with the Axopatch 700B amplifier and
548 pCLAMP 10.4 acquisition software (Molecular Devices). Data were digitized with an analog-to-
549 digital converter (Digidata 1550; Molecular Devices), stored on a personal computer with a data

550 acquisition program (ClampeX version 10.4; Molecular Devices), and analyzed with a software
551 package (Clampfit version 10.7; Molecular Devices). Spontaneous inhibitory postsynaptic
552 currents (sIPSCs) were recorded in the voltage-clamp mode at a holding potential of 0 mV. Patch
553 pipettes were filled with an internal solution (120 mM $CsMeSO_4$, 15 mM CsCl, 10 mM HEPES,
554 5 mM QX-314, 4 mM MgATP, 0.3 mM Na_2GTP, 0.2 mM EGTA, 10 mM TEA-Cl and 8 mM
555 NaCl [pH 7.28] adjusted with CsOH), and whole-cell patch-clamp recordings were made from
556 SG neurons. Resting membrane potentials (RMPs) were recorded in current-clamp mode. Patch
557 pipettes were filled with an internal solution (125 mM K-gluconate, 10 mM KCl, 0.5 mM EGTA,
558 10 mM HEPES, 4 mM ATP-Mg, 0.3 mM NaGTP, 10 mM phosphocreatine, pH 7.28 adjusted
559 with KOH), and whole-cell patch-clamp recordings were made from $tdTomato^+$ or $mCherry^+$
560 neurons. The following drugs were used: NA (20 μM; #74480; Sigma-Aldrich), clozapine-N-
561 oxide (CNO; 100 μM; #BML-NS105; Enzo Life Sciences), CPT (1 μM), N6-
562 Cyclopentyladenosine (CPA; 1 μM; #119135; Sigma-Aldrich), CNQX disodium salt hydrate
563 (CNQX; 10 μM; #C239; Sigma-Aldrich), (+)-MK-801 hydrogen maleate (MK-801; 20 μM;
564 #M107; Sigma-Aldrich), 1(S), 9(R)-(-)-bicuculline methiodide (10 μM; #14340; Sigma-Aldrich)
565 and strychnine (1 μM; #S0532; Sigma-Aldrich). All drugs were dissolved in aCSF solution. CNO
566 was superfused for 3 min. Bath application of CPT was continuously superfused from 4 min
567 before CNO application. NA was superfused with an antagonist cocktail (CNQX, MK-801,
568 bicuculline and strychnine) for 3–5 min. If the recording neuron was depolarized by NA
569 perfusion, then CPA was co-perfused with NA and an antagonist cocktail for 3 min. The
570 frequency of sIPSCs for 1 min of pre- and post-NA application were quantified using Clampfit
571 version 10.7 (Molecular Devices). We quantified averaged RMP for 1 min of pre- and post-drug
572 application, and a change in RMP (ΔRMP) of 5 mV or more was judged to be depolarization or
573 hyperpolarization.

574 ***In situ* hybridization:** Mice were deeply anesthetized with an i.p. injection of pentobarbital and
575 transcardially perfused with PBS followed by ice-cold 4% PFA/PBS. The L4 spinal cord was
576 removed and postfixed in the same fixative 24 hours at 4°C. After that, tissues were incubated
577 with 10%, 20% and 30% sucrose solutions at 4°C, embedded in OCT compound, and stored at
578 −25°C before use. The L4 segments were sectioned at a thickness of 14 μm. *In situ* hybridization
579 was performed using RNAscope® Multiplex Fluorescent Reagent Kit v2 (#323100; ACDbio),
580 according to the manufacture's protocol for fixed frozen tissue. The following probes were used:
581 Mm-Adora1 (#402261; ACDbio); Mm-Slc32a1-C3 (#319191-C3; ACDbio). Tissue sections were

582 analyzed using an LSM700 Imaging System. Cells were considered positive if three or more
583 punctate dots were present in the nucleus and/or cytoplasm[14].

584 **Electrical stimulation of Aβ fibers and counting of pERK$^+$ neurons in the SDH:** After
585 exposure to 1-hour restraint stress, mice were deeply anesthetized with an i.p. injection of
586 urethane (1.2–1.5 mg/kg). Thirty min after stress, Aβ fiber stimulation was performed. The
587 electrodes were attached to the plantar and dorsal surfaces of the left hindpaw. Transcutaneous
588 nerve stimuli were applied using a stimulus generator (#STG4002-16 mA; Multi Channel
589 Systems). The current intensity of the 2,000-Hz stimuli was 1,000 μA[52]. Mice were fixed at 2 min
590 after electrical stimulation. For quantification of pERK$^+$ cells, three sections from the L4 spinal
591 cord segments were randomly selected from each mouse, and the number of pERK$^+$ neurons in
592 the superficial laminae I–IIi (defined by staining of IB4) was counted. Consistent with a previous
593 study[52], we confirmed that electrical stimulation of Aδ and C fibers, but not Aβ fibers, induced
594 ERK phosphorylation in SDH neurons (data not shown).

595 **Statistical analysis:** Statistical analyses were performed using Prism (GraphPad). Quantitative
596 data were expressed as the mean ± SEM. Statistical significance of differences was determined by
597 using two-tailed paired *t*-test (Figure. S1), Mann-Whitney test (Figure. 2F), Wilcoxon signed-
598 rank test (Figure. 3L and 3N), Friedman test with Dunn's multiple comparisons test (Figure. 1E
599 and 2E), one-way ANOVA with Dunnett's multiple comparisons test (Figure. 2C), one-way
600 ANOVA with Tukey's multiple comparisons test (Figure. 4F) and repeated measures two-way
601 ANOVA with Bonferroni's multiple comparisons test (Figure. 1B, 1H, 1K, 1N, 2G, 2H, 2I, 2J,
602 3A, 3B, 3C, 4A, 4B, 4C and 4D). P values are indicated as $*P < 0.05$, $**P < 0.01$, $***P < 0.001$,
603 $****P < 0.0001$.

604

Acknowledgments: We would like to thank Editage for editing a draft of this manuscript, and the University of Pennsylvania vector core for providing pZac2.1, pAAV2/5, pAAV2/9 and pAd DeltaF6 plasmid. Some figure elements were created with BioRender.com. This work was supported by Japan Society for the Promotion of Science (JSPS) KAKENHI Grants JP19H05658 (M.T.), JP20H05900 (M.T.) and JP24H00067 (M.T.), by the Core Research for Evolutional Science and Technology (CREST) program from AMED under Grant Number 24gm1510013h (M.T.), and by Research Support Project for Life Science and Drug Discovery (Basis for Supporting Innovative Drug Discovery and Life Science Research (BINDS)) from AMED under Grant Number JP24ama121031 (M.T.). R.K-K., S.U., and K.Y. were JSPS research fellows (JP22KJ2471, JP23KJ1729, and JP19J21063, respectively).

Author contributions:

Conceptualization: MT

Formal analysis: RKK, SU, KY

Funding acquisition: RKK, SU, KY, MT

Investigation: RKK, SU, KY, DK

Methodology: RKK, SU, KY, KM, KFT

Project administration: MT

Resources: TM, IH

Supervision: MT

Visualization: RKK, SU, MT

Writing–original draft: RKK, SU, KY, MT

Writing–review and editing: RKK, SU, MT

Declaration of interests: The authors declare no competing interests.

Data and materials availability: All data associated with this study are present in the paper or the Supplemental Information.

Figures and figure legends

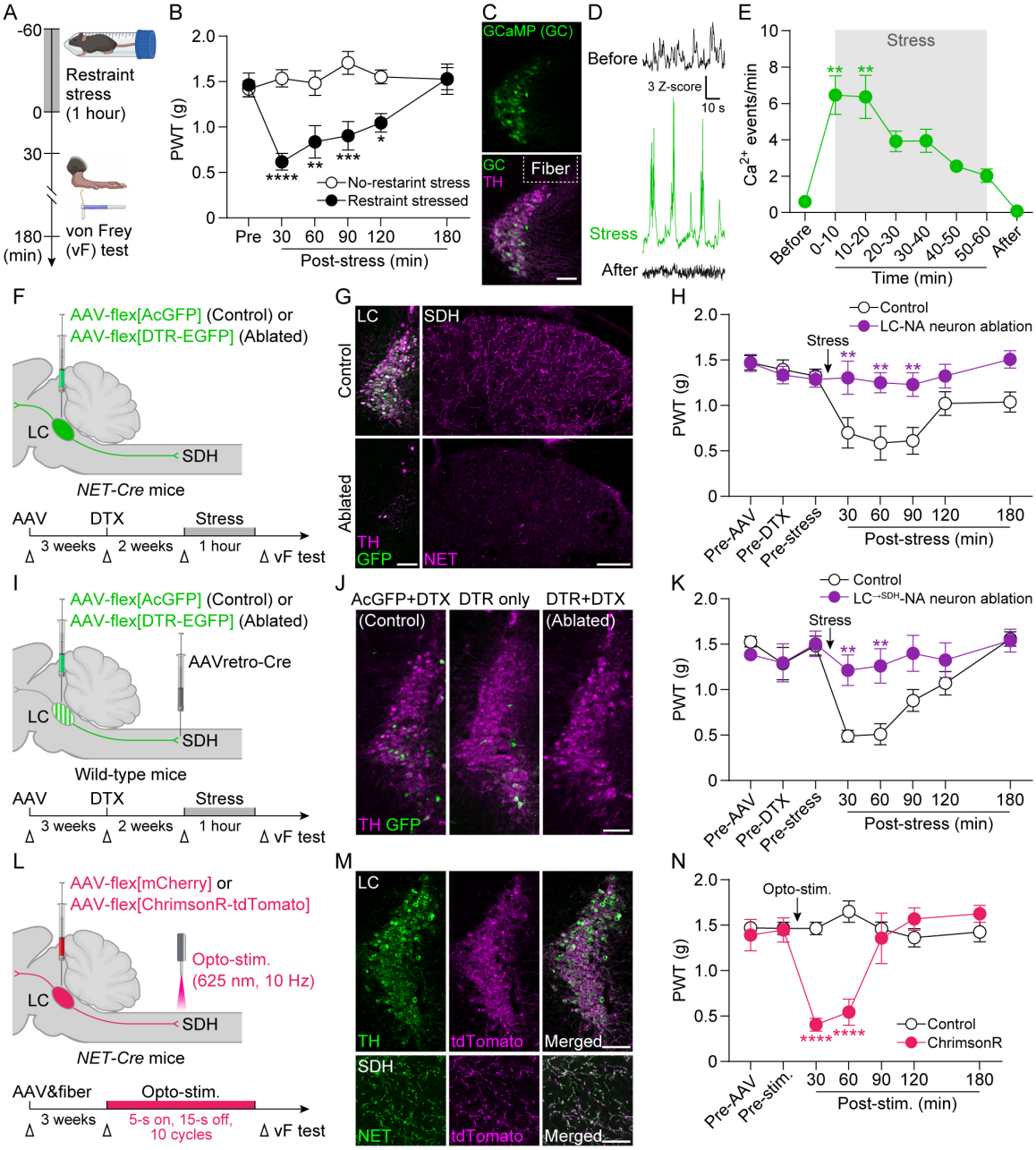

Figure 1. LC→SDH-NA neurons mediate stress-induced mechanical hypersensitivity.

(A) Schematic illustration of an experiment to investigate the effects of acute exposure to restraint stress (1 hour) on mechanosensory behavior in mice, using von Frey (vF) filaments. (B) Change in paw withdrawal threshold (PWT) measured by vF filaments in wild-type mice after restraint stress (n = 6 mice per group; two-way ANOVA with post hoc Bonferroni's multiple comparisons test; *P < 0.05, **P < 0.01, ***P < 0.001, ****P <0.0001 vs. no-restraint stress group). (C) Expression of GCaMP6s (GC; green) in the LC at 3 weeks after intra-LC injection of AAV-flex[GCaMP6s] in *NET-Cre* mice. TH immunofluorescence is shown in magenta. Dashed line indicates the location of the implanted optic fiber. Scale bar, 100 μm. (D

641 and E) Representative traces and change in the frequency of GCaMP6s signals in LC-NA neurons (n = 6
642 mice; Friedman test with post hoc Dunn's multiple comparisons test; **P < 0.01 vs. the data of 'Before').
643 Traces shown at the top, middle, and bottom (D) indicate Ca^{2+} signals before, during, and after restraint
644 stress, respectively. (F) Schematic illustration of the strategy of ablating LC-NA neurons using AAV
645 vectors incorporating DTR (fused with EGFP) injected into the LC in *NET-Cre* mice. (G) TH
646 immunofluorescence (magenta) and GFP (green) in the LC (left) and NET immunofluorescence (magenta)
647 in the SDH (right) after administration of DTX (10 µg/kg, i.p., two injections 24 h-apart) in control mice
648 (top) and DTR-expressing mice (bottom). Scale bars, 100 µm. (H) Effects of ablation of LC-NA neurons on
649 PWT changes after acute restraint stress (n = 7 mice per group; two-way ANOVA with post hoc
650 Bonferroni's multiple comparisons test; **P < 0.01 vs. control group). (I) Schematic illustration of the
651 strategy of ablating $LC^{\rightarrow SDH}$-NA neurons using a retrograde AAV vector incorporating Cre injected into the
652 SDH and an AAV vector incorporating DTR (fused with EGFP) injected into the LC in wild-type mice. (J)
653 Representative images of $LC^{\rightarrow SDH}$ -NA neurons in control or DTR-expressing mice treated with vehicle or
654 DTX administration, respectively. GFP (green) and TH (magenta). Scale bar, 100 µm. (K) Effect of
655 ablation of $LC^{\rightarrow SDH}$ -NA neurons on PWT changes after restraint stress (n = 11 mice per group; two-way
656 ANOVA with post hoc Bonferroni's multiple comparisons test; **P < 0.01 vs. control group). (L)
657 Schematic illustration of the strategy for activating $LC^{\rightarrow SDH}$-NA neuronal axons/terminals using an AAV
658 vector incorporating ChrimsonR (fused with tdTomato) injected into the LC in *NET-Cre* mice and of an
659 optic cannula implanted in the SDH. (M) Representative images of TH (green) and tdTomato (magenta)
660 expression in the LC (top) and NET (green) and tdTomato (magenta) expression in the SDH (bottom) at 3
661 weeks after intra-LC injection of AAV-flex[ChrimsonR-tdTomato] in *NET-Cre* mice. Scale bars, 100 µm
662 (top) and 50 µm (bottom). (N) PWT before and after optogenetic stimulation (opto-stim.) in $LC^{\rightarrow SDH}$-NA
663 axons/terminals (625 nm, 2 mW, 10 Hz, 5-ms pulse duration, 5-s light on, 15-s light off, 10 cycles)
664 (Control, n = 4 mice; ChrimsonR, n = 5 mice; two-way ANOVA with post hoc Bonferroni's multiple
665 comparisons test; ****P <0.0001 vs. control group). Data represent mean ± SEM. See also Figure S1 and
666 S2.

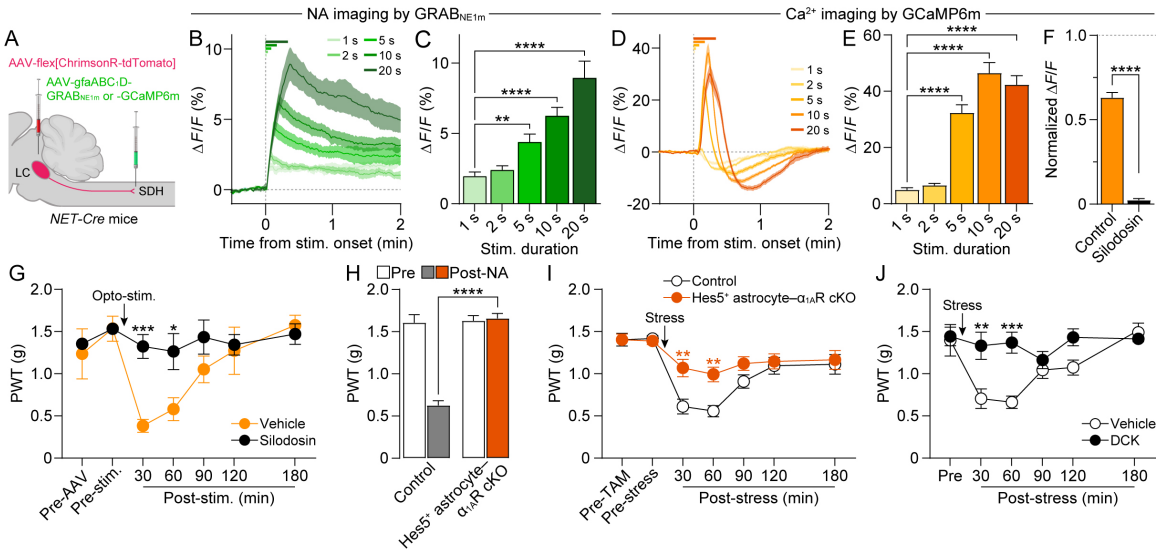

Figure 2. α_{1A}Rs in Hes5$^+$ SDH astrocytes are required for stress-induced mechanical hypersensitivity. (A) Schematic illustration of intra-SDH microinjection of AAV-gfaABC$_1$D-GRAB$_{NE1m}$ or -GCaMP6m and intra-LC microinjection of AAV-flex[ChrimsonR-tdTomato] in *NET-Cre* mice. (B) Representative traces of GRAB$_{NE1m}$ signals by fluorescence imaging using spinal cord slices. Each trace represents the GRAB$_{NE1m}$ signal before and after optogenetic stimulation (625 nm, 1 mW, 10 Hz, 5 ms pulse duration, 1–20 s). (C) Quantitative analysis of the peak amplitude of GRAB$_{NE1m}$ $\Delta F/F$ after optogenetic stimulation in LC$^{\rightarrow SDH}$-NA axons/terminals (n = 4 slices; one-way ANOVA with post hoc Dunnett's multiple comparisons test; $^{**}P < 0.01$, $^{****}P < 0.0001$). (D) Representative traces of astrocytic GCaMP6m signals by fluorescence imaging using spinal cord slices. Each trace represents the GCaMP6m signal before and after optogenetic stimulation (as described in B). (E) Quantitative analysis of the peak amplitude of GCaMP6m $\Delta F/F$ after optogenetic stimulation in LC$^{\rightarrow SDH}$-NA axons/terminals (n = 133 cells, 4 slices, 4 mice; Friedman test with post hoc Dunn's multiple comparisons test; $^{****}P < 0.0001$). (F) Effect of silodosin (40 nM) on astrocytic Ca^{2+} responses in the SDH after optogenetic stimulation (10 s) in LC$^{\rightarrow SDH}$-NA axons/terminals (Control, n = 83 cells, 4 slices, 4 mice; Silodosin, n = 53 cells, 4 slices, 4 mice; Mann-Whitney test; $^{****}P < 0.0001$). (G) Effect of intrathecal silodosin (3 nmol) on mechanical hypersensitivity induced by optogenetic stimulation in LC$^{\rightarrow SDH}$-NA axons/terminals (Vehicle, n = 5 mice; Silodosin, n = 6 mice; two-way ANOVA with post hoc Bonferroni's multiple comparisons test; $^{*}P < 0.05$, $^{***}P < 0.001$ vs. vehicle group). (H) Change in PWT at 30 min after intrathecal injection of NA (0.1 nmol) in control (*Adra1a*$^{flox/flox}$) and Hes5$^+$ astrocyte-selective α_{1A}R conditional knockout mice [*Hes5-CreERT2*;*Adra1a*$^{flox/flox}$ mice treated with tamoxifen (TAM) (Hes5$^+$ astrocyte–α_{1A}R cKO mice) (n = 6 mice per group; two-way ANOVA with post hoc Bonferroni's multiple comparisons test; $^{****}P < 0.0001$). (I and J) Stress-induced mechanical hypersensitivity in Hes5$^+$ astrocyte–α_{1A}R cKO mice [I: Control (*Adra1a*$^{flox/flox}$), n = 7 mice; Hes5$^+$ astrocyte–α_{1A}R cKO, n = 8 mice] or wild-type mice with intrathecal

691 DCK (10 nmol) (J: $n = 5$ mice per group) (two-way ANOVA with post hoc Bonferroni's multiple
692 comparisons test; $^{**}P < 0.01$, $^{***}P < 0.001$ vs. control or vehicle group). Data represent mean ± SEM.

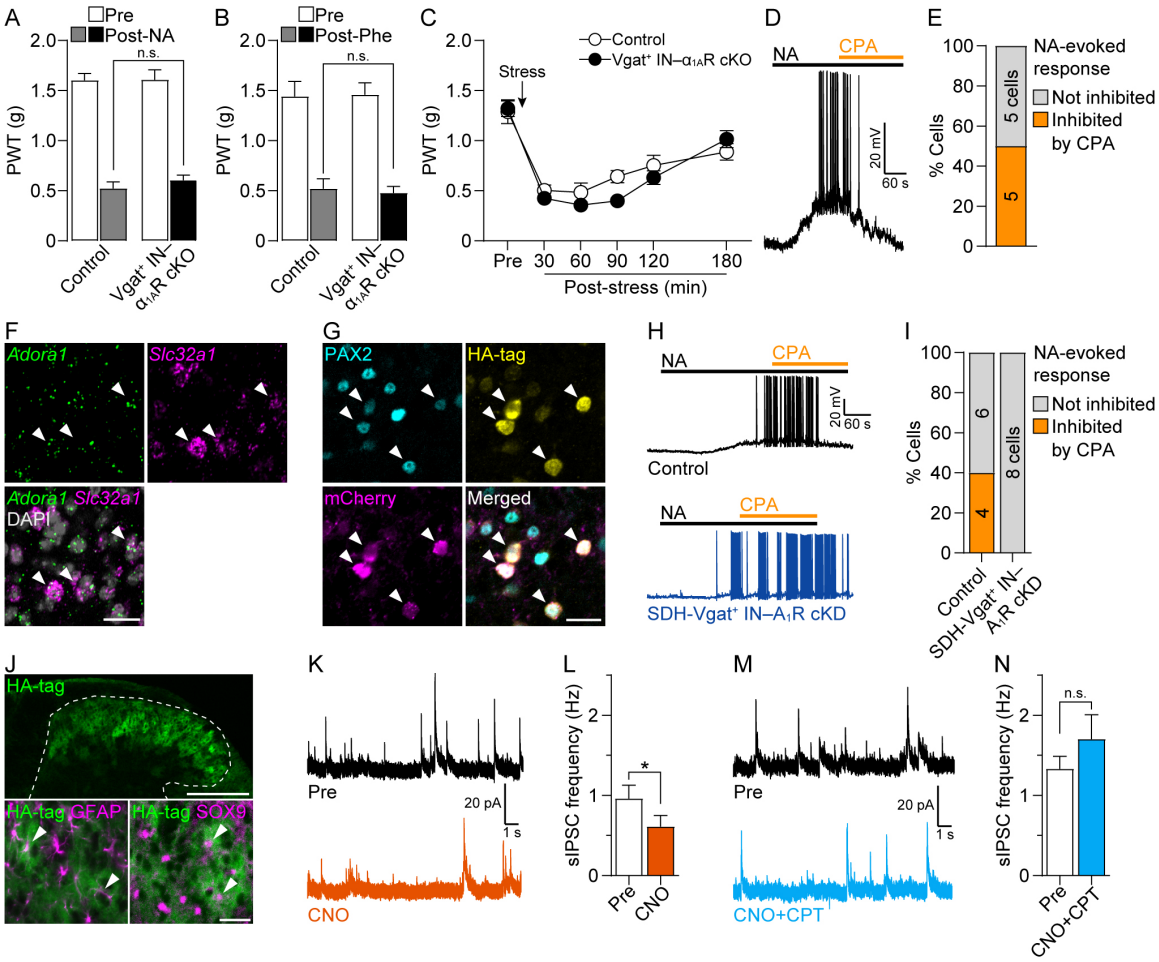

Figure 3. Activation of Hes5$^+$ astrocytes reduces activity in Vgat$^+$ INs in the SDH.

(A and B) Intrathecal NA (A, 0.1 nmol) or Phe (B, 0.05 nmol)-induced mechanical hypersensitivity in control (*Adra1a*$^{flox/flox}$) and Vgat$^+$ IN-selective α_{1A}R conditional knockout mice [*Vgat-Cre*;*Adra1a*$^{flox/flox}$ mice (Vgat$^+$ INs–α_{1A}R cKO mice)] (n = 6 mice per group; two-way ANOVA with post hoc Bonferroni's multiple comparisons test; n.s., not significant). (C) Changes in PWT after acute exposure to restraint stress in control (*Adra1a*$^{flox/flox}$; *n* = 6 mice) and Vgat$^+$ INs–α_{1A}R cKO mice (*n* = 9 mice) (two-way ANOVA with post hoc Bonferroni's multiple comparisons test). (D) Representative trace of membrane potentials in tdTomato$^+$ (Vgat$^+$) SDH neurons after application of NA (20 μM) to spinal cord slices from *Vgat-Cre*;*Rosa-tdTomato* mice. A_1R agonist CPA (1 μM) was co-applied with NA. (E) Percentage of Vgat$^+$ SDH neurons whose NA-evoked response was inhibited by CPA (*n* = 10 cells from 7 mice). (F) Representative images of *Adora1* (A_1R) mRNA expression (green) in *Slc32a1* (Vgat)$^+$ INs (magenta). DAPI staining is shown in gray. Arrowheads indicate A_1R-expressing Vgat$^+$ cells. Scale bar, 25 μm. (G) SaCas9 (yellow, detected by HA-tag) and mCherry (magenta) expression in the PAX2$^+$ INs (cyan) at 3 weeks after intra-SDH injection of AAV-flex[SaCas9] and AAV-flex[mCherry]-U6-sgAdora1 in *Vgat-Cre* mice. Arrowheads indicate genome-editing Vgat$^+$ cells. Scale bar, 25 μm. (H) Representative traces of membrane potentials in Vgat$^+$ INs after application of NA and CPA to spinal cord slices from *Vgat-Cre* mice with

710 conditional knockdown of A_1Rs in *Vgat*$^+$ INs (SDH-Vgat$^+$ IN–A_1R cKD) and their controls (Control; *Vgat-*
711 *Cre* mice with intra-SDH injection of AAV-flex[mCherry]). (I) Percentage of mCherry$^+$ (Vgat$^+$) SDH
712 neurons whose NA-evoked response was inhibited by CPA (Control, n = 10 cells from 8 mice; SDH-Vgat$^+$
713 IN–A_1R cKD, n = 8 cells from 5 mice). (J) Expression of hM3Dq (green, detected by HA-tag) in the SDH
714 at 3 weeks after intra-SDH injection of AAV-flex[hM3Dq] in *Hes5-CreERT2* mice treated with TAM.
715 Dashed line indicates an outline of the gray matter of SDH. GFAP (magenta, bottom left), SOX9 (magenta,
716 bottom right). Arrowheads indicate HA-tag$^+$ astrocytes. Scale bars, 200 μm (top) and 25 μm (bottom). (K
717 and L) Representative traces of sIPSCs (K) and quantitative analysis of their frequency (L) in SG neurons
718 in spinal cord slices from *Hes5-CreERT2*;AAV-hM3Dq mice treated with TAM [Pre and CNO: before and
719 after bath application of CNO (100 μM), respectively] (n = 7 cells from 7 mice; Wilcoxon signed-rank test;
720 *P < 0.05). (M and N) Representative traces of sIPSCs (M) and quantitative analysis of their frequency (N)
721 in SG neurons in spinal cord slices from *Hes5-CreERT2*;AAV-flex[hM3Dq] mice treated with TAM [Pre
722 and CNO: before and after bath application of CNO with CPT (1 μM), respectively] (n = 13 cells from 13
723 mice; Wilcoxon signed-rank test; n.s., not significant). Data represent mean ± SEM.
724

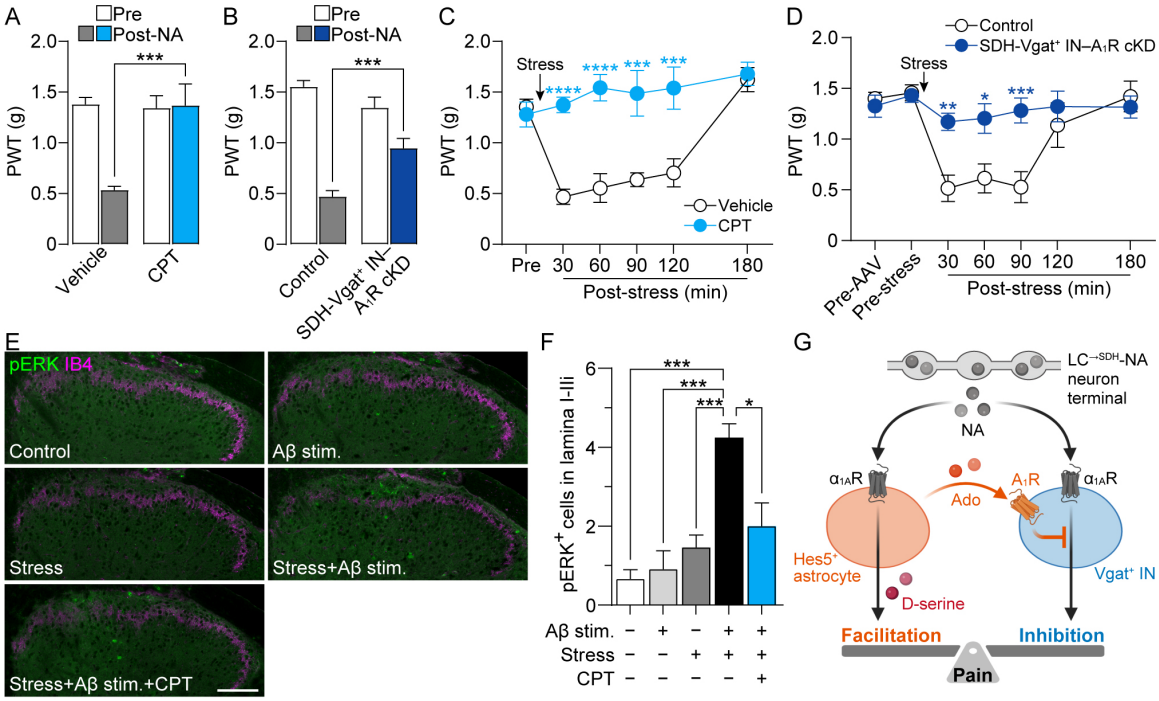

Figure 4. Hes5$^+$ astrocyte-mediated inhibitory signals to SDH-Vgat$^+$ INs contribute to stress-induced mechanical hypersensitivity.

(A and B) PWT before and 30 min after intrathecal administration of NA (0.1 nmol) in wild-type mice pretreated intrathecally with vehicle or CPT (3 nmol) (A: n = 5 mice per group) or in control (*Vgat-Cre* mice with intra-SDH of AAV-flex[mCherry]) and SDH-Vgat$^+$ IN–A$_1$R cKD mice (B: n = 9 mice per group) (two-way ANOVA with post hoc Bonferroni's multiple comparisons test; ***P < 0.001). (C and D) PWT before and after acute restraint stress in wild-type mice pretreated intrathecally with vehicle or CPT (C: Vehicle, n = 6 mice; CPT, n = 5 mice) or in control (*Vgat-Cre* mice with intra-SDH of AAV-flex[mCherry]) and SDH-Vgat$^+$ IN–A$_1$R cKD mice (D: Control, n = 6 mice; SDH-Vgat$^+$ IN–A$_1$R cKD, n = 7 mice) (two-way ANOVA with post hoc Bonferroni's multiple comparisons test; *P < 0.05, **P < 0.01, ***P < 0.001, ****P <0.0001 vs. vehicle or control group). (E) Representative images of pERK (green) and IB4 (magenta) immunofluorescence in the SDH with or without Aβ fiber stimulation and/or restraint stress. CPT was intrathecally administered 30 min before stress exposure. (F) Quantitative analysis of the number of pERK$^+$ cells in superficial laminae of the SDH in each group (n = 4–5 mice per group; one-way ANOVA with post hoc Tukey's multiple comparisons test; *P < 0.05, ***P < 0.001). (G) Schematic illustration of the mechanisms of stress-induced pain facilitation highlighting NA signals from LC$^{\rightarrow SDH}$-NAergic terminals to Hes5$^+$ astrocytes and Vgat$^+$ INs. Data represent mean ± SEM.

745 **References**

746 1. Todd, A.J. (2010). Neuronal circuitry for pain processing in the dorsal horn. Nat Rev
747 Neurosci *11*, 823-836. 10.1038/nrn2947.
748 2. Peirs, C., and Seal, R.P. (2016). Neural circuits for pain: Recent advances and current
749 views. Science *354*, 578-584. 10.1126/science.aaf8933.
750 3. Koch, S.C., Acton, D., and Goulding, M. (2018). Spinal Circuits for Touch, Pain, and
751 Itch. Annu Rev Physiol *80*, 189-217. 10.1146/annurev-physiol-022516-034303.
752 4. Moehring, F., Halder, P., Seal, R.P., and Stucky, C.L. (2018). Uncovering the Cells and
753 Circuits of Touch in Normal and Pathological Settings. Neuron *100*, 349-360.
754 10.1016/j.neuron.2018.10.019.
755 5. Peirs, C., Dallel, R., and Todd, A.J. (2020). Recent advances in our understanding of the
756 organization of dorsal horn neuron populations and their contribution to cutaneous
757 mechanical allodynia. J Neural Transm (Vienna) *127*, 505-525. 10.1007/s00702-020-
758 02159-1.
759 6. Wang, L.H., Ding, W.Q., and Sun, Y.G. (2022). Spinal ascending pathways for
760 somatosensory information processing. Trends Neurosci *45*, 594-607.
761 10.1016/j.tins.2022.05.005.
762 7. Mercer Lindsay, N., Chen, C., Gilam, G., Mackey, S., and Scherrer, G. (2021). Brain
763 circuits for pain and its treatment. Sci Transl Med *13*, eabj7360.
764 10.1126/scitranslmed.abj7360.
765 8. Nguyen, E., Grajales-Reyes, J.G., Gereau, R.W.t., and Ross, S.E. (2023). Cell type-
766 specific dissection of sensory pathways involved in descending modulation. Trends
767 Neurosci *46*, 539-550. 10.1016/j.tins.2023.04.002.
768 9. Yoshimura, M., and Furue, H. (2006). Mechanisms for the anti-nociceptive actions of the
769 descending noradrenergic and serotonergic systems in the spinal cord. J Pharmacol Sci
770 *101*, 107-117. 10.1254/jphs.crj06008x.
771 10. Llorca-Torralba, M., Borges, G., Neto, F., Mico, J.A., and Berrocoso, E. (2016).
772 Noradrenergic Locus Coeruleus pathways in pain modulation. Neuroscience *338*, 93-113.
773 10.1016/j.neuroscience.2016.05.057.
774 11. Suárez-Pereira, I., Llorca-Torralba, M., Bravo, L., Camarena-Delgado, C., Soriano-Mas,
775 C., and Berrocoso, E. (2022). The Role of the Locus Coeruleus in Pain and Associated
776 Stress-Related Disorders. Biol Psychiatry *91*, 786-797. 10.1016/j.biopsych.2021.11.023.
777 12. Li, J., Wei, Y., Zhou, J., Zou, H., Ma, L., Liu, C., Xiao, Z., Liu, X., Tan, X., Yu, T., and
778 Cao, S. (2022). Activation of locus coeruleus-spinal cord noradrenergic neurons
779 alleviates neuropathic pain in mice via reducing neuroinflammation from astrocytes and
780 microglia in spinal dorsal horn. J Neuroinflammation *19*, 123. 10.1186/s12974-022-
781 02489-9.
782 13. Häring, M., Zeisel, A., Hochgerner, H., Rinwa, P., Jakobsson, J.E.T., Lönnerberg, P., La
783 Manno, G., Sharma, N., Borgius, L., Kiehn, O., et al. (2018). Neuronal atlas of the dorsal
784 horn defines its architecture and links sensory input to transcriptional cell types. Nat
785 Neurosci *21*, 869-880. 10.1038/s41593-018-0141-1.
786 14. Shiraishi, Y., Koga, K., Yamagata, R., Hatada, I., Shiratori-Hayashi, M., and Tsuda, M.
787 (2021). α1A-adrenaline receptors in dorsal horn inhibitory neurons have an inhibitory
788 role in the regulation of chloroquine-induced itch in mice. Mol Brain *14*, 55.
789 10.1186/s13041-021-00768-9.
790 15. Baba, H., Goldstein, P.A., Okamoto, M., Kohno, T., Ataka, T., Yoshimura, M., and
791 Shimoji, K. (2000). Norepinephrine facilitates inhibitory transmission in substantia

792 gelatinosa of adult rat spinal cord (part 2): effects on somatodendritic sites of GABAergic
793 neurons. Anesthesiology *92*, 485-492. 10.1097/00000542-200002000-00031.
794 16. Uchiyama, S., Yoshihara, K., Kawanabe, R., Hatada, I., Koga, K., and Tsuda, M. (2022).
795 Stress-induced antinociception to noxious heat requires α1A-adrenaline receptors of
796 spinal inhibitory neurons in mice. Mol Brain *15*, 6. 10.1186/s13041-021-00895-3.
797 17. Inoue, K., and Tsuda, M. (2018). Microglia in neuropathic pain: cellular and molecular
798 mechanisms and therapeutic potential. Nat Rev Neurosci *19*, 138-152.
799 10.1038/nrn.2018.2.
800 18. Ji, R.R., Donnelly, C.R., and Nedergaard, M. (2019). Astrocytes in chronic pain and itch.
801 Nat Rev Neurosci *20*, 667-685. 10.1038/s41583-019-0218-1.
802 19. Tsuda, M., Masuda, T., and Kohno, K. (2023). Microglial diversity in neuropathic pain.
803 Trends Neurosci *46*, 597-610. 10.1016/j.tins.2023.05.001.
804 20. Sekiguchi, K.J., Shekhtmeyster, P., Merten, K., Arena, A., Cook, D., Hoffman, E., Ngo,
805 A., and Nimmerjahn, A. (2016). Imaging large-scale cellular activity in spinal cord of
806 freely behaving mice. Nat Commun *7*, 11450. 10.1038/ncomms11450.
807 21. Yoshihara, K., Matsuda, T., Kohro, Y., Tozaki-Saitoh, H., Inoue, K., and Tsuda, M.
808 (2018). Astrocytic Ca(2+) responses in the spinal dorsal horn by noxious stimuli to the
809 skin. J Pharmacol Sci *137*, 101-104. 10.1016/j.jphs.2018.04.007.
810 22. Kohro, Y., Matsuda, T., Yoshihara, K., Kohno, K., Koga, K., Katsuragi, R., Oka, T.,
811 Tashima, R., Muneta, S., Yamane, T., et al. (2020). Spinal astrocytes in superficial
812 laminae gate brainstem descending control of mechanosensory hypersensitivity. Nat
813 Neurosci *23*, 1376-1387. 10.1038/s41593-020-00713-4.
814 23. Kawanabe, R., Yoshihara, K., Hatada, I., and Tsuda, M. (2021). Activation of spinal
815 dorsal horn astrocytes by noxious stimuli involves descending noradrenergic signaling.
816 Mol Brain *14*, 79. 10.1186/s13041-021-00788-5.
817 24. Hertz, L., Lovatt, D., Goldman, S.A., and Nedergaard, M. (2010). Adrenoceptors in
818 brain: cellular gene expression and effects on astrocytic metabolism and [Ca(2+)]i.
819 Neurochem Int *57*, 411-420. 10.1016/j.neuint.2010.03.019.
820 25. Bazargani, N., and Attwell, D. (2016). Astrocyte calcium signaling: the third wave. Nat
821 Neurosci *19*, 182-189. 10.1038/nn.4201.
822 26. Batiuk, M.Y., Martirosyan, A., Wahis, J., de Vin, F., Marneffe, C., Kusserow, C.,
823 Koeppen, J., Viana, J.F., Oliveira, J.F., Voet, T., et al. (2020). Identification of region-
824 specific astrocyte subtypes at single cell resolution. Nat Commun *11*, 1220.
825 10.1038/s41467-019-14198-8.
826 27. Wahis, J., Akkaya, C., Kirunda, A.M., Mak, A., Zeise, K., Verhaert, J., Gasparyan, H.,
827 Hovhannisyan, S., and Holt, M.G. (2024). The astrocyte α1A-adrenoreceptor is a key
828 component of the neuromodulatory system in mouse visual cortex. Glia.
829 10.1002/glia.24591.
830 28. Cohen, Z., Molinatti, G., and Hamel, E. (1997). Astroglial and vascular interactions of
831 noradrenaline terminals in the rat cerebral cortex. J Cereb Blood Flow Metab *17*, 894-
832 904. 10.1097/00004647-199708000-00008.
833 29. Valentino, R.J., and Van Bockstaele, E. (2008). Convergent regulation of locus coeruleus
834 activity as an adaptive response to stress. Eur J Pharmacol *583*, 194-203.
835 10.1016/j.ejphar.2007.11.062.
836 30. Imbe, H., Okamoto, K., Donishi, T., Kawai, S., Enoki, K., Senba, E., and Kimura, A.
837 (2009). Activation of ERK in the locus coeruleus following acute noxious stimulation.
838 Brain Res *1263*, 50-57. 10.1016/j.brainres.2009.01.052.

839 31. Chen, F.J., and Sara, S.J. (2007). Locus coeruleus activation by foot shock or electrical
840 stimulation inhibits amygdala neurons. Neuroscience *144*, 472-481.
841 10.1016/j.neuroscience.2006.09.037.
842 32. McCall, J.G., Al-Hasani, R., Siuda, E.R., Hong, D.Y., Norris, A.J., Ford, C.P., and
843 Bruchas, M.R. (2015). CRH Engagement of the Locus Coeruleus Noradrenergic System
844 Mediates Stress-Induced Anxiety. Neuron *87*, 605-620. 10.1016/j.neuron.2015.07.002.
845 33. Butler, R.K., and Finn, D.P. (2009). Stress-induced analgesia. Prog Neurobiol *88*, 184-
846 202. 10.1016/j.pneurobio.2009.04.003.
847 34. Jennings, E.M., Okine, B.N., Roche, M., and Finn, D.P. (2014). Stress-induced
848 hyperalgesia. Prog Neurobiol *121*, 1-18. 10.1016/j.pneurobio.2014.06.003.
849 35. François, A., Low, S.A., Sypek, E.I., Christensen, A.J., Sotoudeh, C., Beier, K.T.,
850 Ramakrishnan, C., Ritola, K.D., Sharif-Naeini, R., Deisseroth, K., et al. (2017). A
851 Brainstem-Spinal Cord Inhibitory Circuit for Mechanical Pain Modulation by GABA and
852 Enkephalins. Neuron *93*, 822-839.e826. 10.1016/j.neuron.2017.01.008.
853 36. Abdallah, C.G., and Geha, P. (2017). Chronic Pain and Chronic Stress: Two Sides of the
854 Same Coin? Chronic Stress (Thousand Oaks) *1*, 2470547017704763.
855 10.1177/2470547017704763.
856 37. Fitzcharles, M.A., Cohen, S.P., Clauw, D.J., Littlejohn, G., Usui, C., and Häuser, W.
857 (2021). Nociplastic pain: towards an understanding of prevalent pain conditions. Lancet
858 *397*, 2098-2110. 10.1016/s0140-6736(21)00392-5.
859 38. Sousa, F.S.S., Birmann, P.T., Balaguez, R., Alves, D., Brüning, C.A., and Savegnago, L.
860 (2018). α-(phenylselanyl) acetophenone abolishes acute restraint stress induced-comorbid
861 pain, depression and anxiety-related behaviors in mice. Neurochem Int *120*, 112-120.
862 10.1016/j.neuint.2018.08.006.
863 39. Wagatsuma, A., Okuyama, T., Sun, C., Smith, L.M., Abe, K., and Tonegawa, S. (2018).
864 Locus coeruleus input to hippocampal CA3 drives single-trial learning of a novel context.
865 Proc Natl Acad Sci U S A *115*, E310-E316. 10.1073/pnas.1714082115.
866 40. Mulvey, B., Bhatti, D.L., Gyawali, S., Lake, A.M., Kriaucionis, S., Ford, C.P., Bruchas,
867 M.R., Heintz, N., and Dougherty, J.D. (2018). Molecular and Functional Sex Differences
868 of Noradrenergic Neurons in the Mouse Locus Coeruleus. Cell Rep *23*, 2225-2235.
869 10.1016/j.celrep.2018.04.054.
870 41. Saito, M., Iwawaki, T., Taya, C., Yonekawa, H., Noda, M., Inui, Y., Mekada, E., Kimata,
871 Y., Tsuru, A., and Kohno, K. (2001). Diphtheria toxin receptor-mediated conditional and
872 targeted cell ablation in transgenic mice. Nat Biotechnol *19*, 746-750. 10.1038/90795.
873 42. Klapoetke, N.C., Murata, Y., Kim, S.S., Pulver, S.R., Birdsey-Benson, A., Cho, Y.K.,
874 Morimoto, T.K., Chuong, A.S., Carpenter, E.J., Tian, Z., et al. (2014). Independent
875 optical excitation of distinct neural populations. Nat Methods *11*, 338-346.
876 10.1038/nmeth.2836.
877 43. Feng, J., Zhang, C., Lischinsky, J.E., Jing, M., Zhou, J., Wang, H., Zhang, Y., Dong, A.,
878 Wu, Z., Wu, H., et al. (2019). A Genetically Encoded Fluorescent Sensor for Rapid and
879 Specific In Vivo Detection of Norepinephrine. Neuron *102*, 745-761.e748.
880 10.1016/j.neuron.2019.02.037.
881 44. Lee, Y., Messing, A., Su, M., and Brenner, M. (2008). GFAP promoter elements required
882 for region-specific and astrocyte-specific expression. Glia *56*, 481-493.
883 10.1002/glia.20622.
884 45. Nam, Y., Kim, J.H., Jha, M.K., Jung, J.Y., Lee, M.G., Choi, I.S., Jang, I.S., Lim, D.G.,
885 Hwang, S.H., Cho, H.J., and Suk, K. (2016). Reversible Induction of Pain
886 Hypersensitivity following Optogenetic Stimulation of Spinal Astrocytes. Cell Rep *17*,
887 3049-3061. 10.1016/j.celrep.2016.11.043.

46. Metzner, K., Gross, T., Balzulat, A., Wack, G., Lu, R., and Schmidtko, A. (2021). Lack of efficacy of a partial adenosine A1 receptor agonist in neuropathic pain models in mice. Purinergic Signal *17*, 503-514. 10.1007/s11302-021-09806-6.
47. Cui, X., Liu, J., Uniyal, A., Xu, Q., Zhang, C., Zhu, G., Yang, F., Sivanesan, E., Linderoth, B., Raja, S.N., and Guan, Y. (2024). Enhancing spinal cord stimulation-induced pain inhibition by augmenting endogenous adenosine signalling after nerve injury in rats. Br J Anaesth *132*, 746-757. 10.1016/j.bja.2024.01.005.
48. Ran, F.A., Cong, L., Yan, W.X., Scott, D.A., Gootenberg, J.S., Kriz, A.J., Zetsche, B., Shalem, O., Wu, X., Makarova, K.S., et al. (2015). In vivo genome editing using Staphylococcus aureus Cas9. Nature *520*, 186-191. 10.1038/nature14299.
49. Cheng, L., Arata, A., Mizuguchi, R., Qian, Y., Karunaratne, A., Gray, P.A., Arata, S., Shirasawa, S., Bouchard, M., Luo, P., et al. (2004). Tlx3 and Tlx1 are post-mitotic selector genes determining glutamatergic over GABAergic cell fates. Nat Neurosci *7*, 510-517. 10.1038/nn1221.
50. Roth, B.L. (2016). DREADDs for Neuroscientists. Neuron *89*, 683-694. 10.1016/j.neuron.2016.01.040.
51. Ji, R.R., Baba, H., Brenner, G.J., and Woolf, C.J. (1999). Nociceptive-specific activation of ERK in spinal neurons contributes to pain hypersensitivity. Nat Neurosci *2*, 1114-1119. 10.1038/16040.
52. Matsumoto, M., Xie, W., Ma, L., and Ueda, H. (2008). Pharmacological switch in Abeta-fiber stimulation-induced spinal transmission in mice with partial sciatic nerve injury. Mol Pain *4*, 25. 10.1186/1744-8069-4-25.
53. Kawabata, R., Yamanaka, H., Kobayashi, K., Oke, Y., Fujita, A., Oku, Y., Yao, I., and Koga, K. (2023). The Anterior Cingulate Cortex is Critical for Acute Stress-induced Hypersensitivity in Mice. Neuroscience *523*, 47-60. 10.1016/j.neuroscience.2023.05.010.
54. Hickey, L., Li, Y., Fyson, S.J., Watson, T.C., Perrins, R., Hewinson, J., Teschemacher, A.G., Furue, H., Lumb, B.M., and Pickering, A.E. (2014). Optoactivation of locus ceruleus neurons evokes bidirectional changes in thermal nociception in rats. J Neurosci *34*, 4148-4160. 10.1523/jneurosci.4835-13.2014.
55. Hirschberg, S., Li, Y., Randall, A., Kremer, E.J., and Pickering, A.E. (2017). Functional dichotomy in spinal- vs prefrontal-projecting locus coeruleus modules splits descending noradrenergic analgesia from ascending aversion and anxiety in rats. Elife *6*, e29808. 10.7554/eLife.29808.
56. Duan, B., Cheng, L., Bourane, S., Britz, O., Padilla, C., Garcia-Campmany, L., Krashes, M., Knowlton, W., Velasquez, T., Ren, X., et al. (2014). Identification of spinal circuits transmitting and gating mechanical pain. Cell *159*, 1417-1432. 10.1016/j.cell.2014.11.003.
57. Petitjean, H., Pawlowski, S.A., Fraine, S.L., Sharif, B., Hamad, D., Fatima, T., Berg, J., Brown, C.M., Jan, L.Y., Ribeiro-da-Silva, A., et al. (2015). Dorsal Horn Parvalbumin Neurons Are Gate-Keepers of Touch-Evoked Pain after Nerve Injury. Cell Rep *13*, 1246-1257. 10.1016/j.celrep.2015.09.080.
58. Wang, H., Chen, W., Dong, Z., Xing, G., Cui, W., Yao, L., Zou, W.J., Robinson, H.L., Bian, Y., Liu, Z., et al. (2022). A novel spinal neuron connection for heat sensation. Neuron *110*, 2315-2333.e2316. 10.1016/j.neuron.2022.04.021.
59. Warwick, C., Salsovic, J., Hachisuka, J., Smith, K.M., Sheahan, T.D., Chen, H., Ibinson, J., Koerber, H.R., and Ross, S.E. (2022). Cell type-specific calcium imaging of central sensitization in mouse dorsal horn. Nat Commun *13*, 5199. 10.1038/s41467-022-32608-2.

935 60. Torsney, C., and MacDermott, A.B. (2006). Disinhibition opens the gate to pathological
936 pain signaling in superficial neurokinin 1 receptor-expressing neurons in rat spinal cord. J
937 Neurosci *26*, 1833-1843. 10.1523/jneurosci.4584-05.2006.
938 61. Sonohata, M., Doi, A., Yasaka, T., Uta, D., Mawatari, M., and Yoshimura, M. (2019).
939 Noradrenaline modulates mechanically evoked responses in the rat spinal dorsal horn: an
940 in vivo patch-clamp study. J Pain Res *12*, 1269-1278. 10.2147/jpr.s181210.
941 62. Pankratov, Y., and Lalo, U. (2015). Role for astroglial α1-adrenoreceptors in
942 gliotransmission and control of synaptic plasticity in the neocortex. Front Cell Neurosci
943 *9*, 230. 10.3389/fncel.2015.00230.
944 63. Xu, Q., Ford, N.C., He, S., Huang, Q., Anderson, M., Chen, Z., Yang, F., Crawford, L.K.,
945 Caterina, M.J., Guan, Y., and Dong, X. (2021). Astrocytes contribute to pain gating in the
946 spinal cord. Sci Adv *7*, eabi6287. 10.1126/sciadv.abi6287.
947 64. Oe, Y., Wang, X., Patriarchi, T., Konno, A., Ozawa, K., Yahagi, K., Hirai, H., Tsuboi, T.,
948 Kitaguchi, T., Tian, L., et al. (2020). Distinct temporal integration of noradrenaline
949 signaling by astrocytic second messengers during vigilance. Nat Commun *11*, 471.
950 10.1038/s41467-020-14378-x.
951 65. Lerman, S.F., Rudich, Z., Brill, S., Shalev, H., and Shahar, G. (2015). Longitudinal
952 associations between depression, anxiety, pain, and pain-related disability in chronic pain
953 patients. Psychosom Med *77*, 333-341. 10.1097/psy.0000000000000158.
954 66. Lugert, S., Vogt, M., Tchorz, J.S., Müller, M., Giachino, C., and Taylor, V. (2012).
955 Homeostatic neurogenesis in the adult hippocampus does not involve amplification of
956 Ascl1(high) intermediate progenitors. Nat Commun *3*, 670. 10.1038/ncomms1670.
957 67. Vong, L., Ye, C., Yang, Z., Choi, B., Chua, S., Jr., and Lowell, B.B. (2011). Leptin
958 action on GABAergic neurons prevents obesity and reduces inhibitory tone to POMC
959 neurons. Neuron *71*, 142-154. 10.1016/j.neuron.2011.05.028.
960 68. Madisen, L., Zwingman, T.A., Sunkin, S.M., Oh, S.W., Zariwala, H.A., Gu, H., Ng, L.L.,
961 Palmiter, R.D., Hawrylycz, M.J., Jones, A.R., et al. (2010). A robust and high-throughput
962 Cre reporting and characterization system for the whole mouse brain. Nat Neurosci *13*,
963 133-140. 10.1038/nn.2467.
964 69. Chaplan, S.R., Bach, F.W., Pogrel, J.W., Chung, J.M., and Yaksh, T.L. (1994).
965 Quantitative assessment of tactile allodynia in the rat paw. J Neurosci Methods *53*, 55-63.
966 10.1016/0165-0270(94)90144-9.
967 70. Kohro, Y., Sakaguchi, E., Tashima, R., Tozaki-Saitoh, H., Okano, H., Inoue, K., and
968 Tsuda, M. (2015). A new minimally-invasive method for microinjection into the mouse
969 spinal dorsal horn. Sci Rep *5*, 14306. 10.1038/srep14306.
970 71. Zhang, Z.M., Chen, S., and Liang, Y.Z. (2010). Baseline correction using adaptive
971 iteratively reweighted penalized least squares. Analyst *135*, 1138-1146.
972 10.1039/b922045c.
973 72. Thévenaz, P., Ruttimann, U.E., and Unser, M. (1998). A pyramid approach to subpixel
974 registration based on intensity. IEEE Trans Image Process *7*, 27-41. 10.1109/83.650848.

Supplemental Information for

Descending locus coeruleus noradrenergic signaling to spinal astrocyte subset is required for stress-induced pain facilitation

Riku Kawanabe-Kobayashi[1,8], Sawako Uchiyama[1,8], Kohei Yoshihara[1,8], Daiki Kojima[1], Thomas McHugh[2], Izuho Hatada[3,4], Ko Matsui[5], Kenji F. Tanaka[6], Makoto Tsuda[1,7,*]

*Corresponding author:
Makoto Tsuda, Ph.D.
Email: tsuda@phar.kyushu-u.ac.jp

This PDF file includes:

Figures S1 and S2

Supplemental Figures

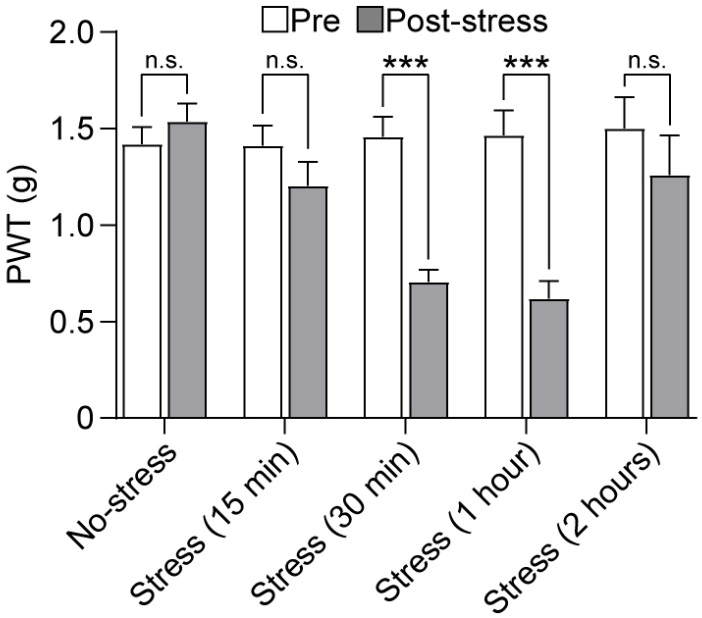

Figure S1. Mechanical hypersensitivity is weak in mice with longer exposure (2 hours) to restraint stress.

PWT change at 30 min after various exposure periods of restraint stress (15 min, 30 min, 1 hour, and 2 hours) in wild-type mice (n = 5 mice; two-tailed paired t-test; ***P < 0.001; n.s., not significant vs. pre group). Data represent mean ± SEM.

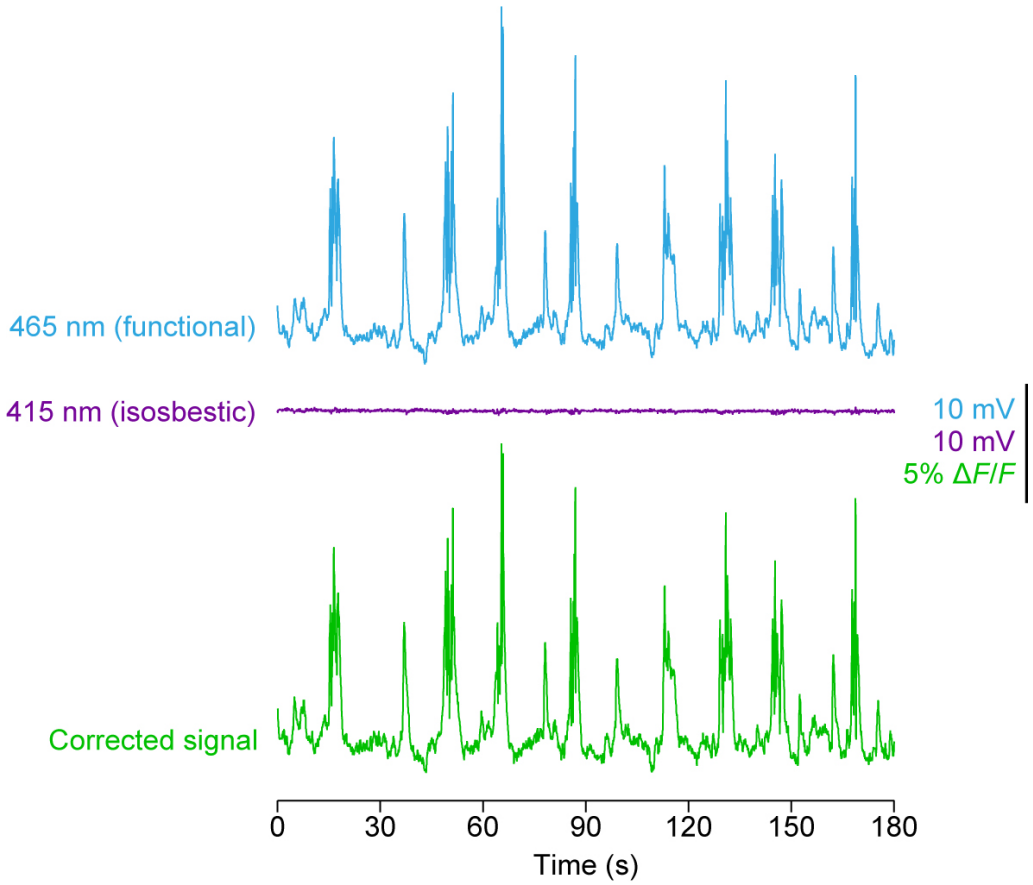

Figure S2. Raw fluorescent signals in LC-NA neurons during restraint stress (in vivo fiber photometry).

Representative traces of GCaMP6s signals in LC-NA neurons during restraint stress. Traces shown at the top (blue), middle (purple), and bottom (green) indicate 465-nm, 415-nm, and corrected fluorescent signals, respectively.